CRC Report No. A-118

ROLE OF METEOROLOGY, EMISSIONS AND SMOKE ON OZONE IN THE SOUTH COAST AIR BASIN

Final Report

January 2020

COORDINATING RESEARCH COUNCIL, INC.
5755 NORTH POINT PARKWAY • SUITE 265 • ALPHARETTA, GA 30022

The Coordinating Research Council, Inc. (CRC) is a non-profit corporation supported by the petroleum and automotive equipment industries. CRC operates through the committees made up of technical experts from industry and government who voluntarily participate. The four main areas of research within CRC are: air pollution (atmospheric and engineering studies); aviation fuels, lubricants, and equipment performance; heavy-duty vehicle fuels, lubricants, and equipment performance (e.g., diesel trucks); and light-duty vehicle fuels, lubricants, and equipment performance (e.g., passenger cars). CRC's function is to provide the mechanism for joint research conducted by the two industries that will help in determining the optimum combination of petroleum products and automotive equipment. CRC's work is limited to research that is mutually beneficial to the two industries involved. The final results of the research conducted by, or under the auspices of, CRC are available to the public.

Role of meteorology, emissions and smoke on O_3 in the South Coast air basins

CRC Project A-118

By Dr. Dan Jaffe

School of Science, Technology, Engineering and Mathematics

University of Washington Bothell

Bothell, WA 98011

Executive summary

The Los Angeles/Riverside/South Coast airshed has the highest O_3 design value (ODV) in the country and is home to approximately 18 million people. While maximum daily 8-hour average (MDA8) O_3 concentrations have declined substantially from the extremely high values seen in the 1980-2000 period, since 2010 there has been little improvement in the O_3 concentrations, despite substantial reductions in the emissions of O_3 precursors. The focus of this project was to understand possible causes for this lack of improvement. In this project I considered three possible explanations:

1. Recent O_3 concentrations have been enhanced due to changes in the photochemical environment as a result of changes in the VOC/NOx ratio. (VOC is volatile organic compounds and NOx is sum of nitric oxide plus nitrogen dioxide).
2. Recent O_3 concentrations have been enhanced due to an increase in the occurrence of wildfire smoke in the region.
3. Recent O_3 concentrations have been enhanced due to increased temperatures in the region, either due to random variations or climate change.

To evaluate these hypotheses, I used a variety of tools including analysis of the observed O_3 and NOx patterns, development of Generalized Additive Models (GAMs) and analysis of long-term meteorological data in the region. The time period of this analysis focused on 2000-2018. The GAMs were developed using data for 2006-2018. From this analysis, I found that in the early part of this period (2006-2008), the highest number of high O_3 days was on weekends, when NOx concentrations were lowest, however this has now shifted. At present, the greatest frequency of high O_3 days is on weekdays. Sunday now has the fewest high O_3 days and is the day with the lowest NOx concentrations. As NOx concentrations have declined on all days, this suggests that Sundays have transitioned to a NOx limited regime and weekdays are now near the optimum VOC/NOx ratio for O_3 production. NOx concentrations steadily declined until 2013, but have stagnated since then. This is in contrast to the emission inventory (EI) which shows a steady decline thru 2018. Between 2014 and 2018 the EI shows a 20% reduction whereas surface and satellite observations of NO_2 show essentially no change. This suggests that emissions have not declined since 2014.

As part of this project I developed and used GAMs to model and predict the MDA8 O_3 concentrations in the South Coast airshed. The R^2 for the GAM predictions range from 0.67 to 0.76, depending on site. The GAM has a lower predictive power for the background Vandenberg AFB site ($R^2 = 0.53$), where concentrations are lower and local O_3 production is less important. Due to the changing photochemical environment, inclusion of interaction terms between predictors improves the GAM performance. I then used the GAMs to examine O_3 on smoke influenced days. To identify days with smoke influence, I used a combination of the satellite derived NOAA Hazard Mapping System- Fire and Smoke Product, combined with surface $PM_{2.5}$

concentrations. However relatively high $PM_{2.5}$ in the airshed makes it difficult to clearly identify fire influence at the lower elevation (basin) sites, compared to the elevated Crestline site. Thus impacts on the MDA8 O_3 due to smoke can only be confidently detected at the Crestline site. At Crestline, the mean residual or extra O_3 due to smoke is 5.6 ppb for the MDA8. In 2016-2018, there were 29 detectable smoke days at Crestline. However even if all 29 days were excluded from consideration, the 2016-2018 design value would only change from 111 to 108 ppb. Thus while we can say that smoke has a modest influence on the MDA8 at Crestline, it does not appear to be a primary driver for the lack of decline in the ODV for the South Coast airshed.

Daily max temperature (DMT) is an important driver for the daily variations in the MDA8, and due to climate change, the DMT is increasing by about 0.02^oC/year. This increase is consistent across the mean, 95^{th} and 98^{th} percentiles of the annual DMT values. This will increase the average MDA8 value by 0.06-0.08 ppb per year or 0.6-0.8 ppb per decade, which will have a modest influence on the ODV. So while climate change is an important long-term consideration for future air quality, at present it has had only a minor impact on the region's ability to meet the National Ambient Air Quality Standards (NAAQS).

The recent reductions in the frequency of high O_3 days seen on Sundays, the day with the lowest NOx concentrations, demonstrates that continued NOx reductions are needed to reduce the ODV in the South Coast airshed. Weekday NOx levels are now similar to what they were on weekends 15 years ago and this is near the optimum VOC/NOx ratio for O_3 production. Given the strong decline in VOCs over the past several decades and the fact that biogenic VOCs are now a significant fraction of the total emissions, further reductions in the ODV will likely only occur when NOx emissions are further reduced. Future research should focus on understanding the cause for the lack of decline in NOx concentrations since 2014.

Table of contents

List of figures

List of tables

1. Introduction

The Los Angeles-Long Beach-Anaheim and Riverside-San Bernardino-Ontario Metropolitan Statistical Areas (MSAs) are home to approximately 18 million people. While great progress has been made on reducing O_3 in the region, levels are still well above the National Ambient Air Quality Standards (NAAQS) and the region currently has the highest O_3 design values (ODV) in the country. However over the past decade there has been little progress in reducing the annual 4th highest Maximum Daily 8-hour Average (MDA8) O_3 concentrations, which is the basis for the policy relevant metric the ODV. Figure 1 shows daily MDA8 and annual 4^{th} highest values from two of the highest sites in the region (Riverside and San Bernardino).

The key ingredients in O_3 production are nitrogen oxides ($NO+NO_2 = NO_x$) and Volatile Organic Compounds (VOCs). The California Air Resources Board compiles information on NOx and VOCs emissions from mobile, stationary and area sources. For VOCs, these are separated into Total Organic Gases (TOGs) and Reactive Organic Gases (ROGs), with the ROGs typically more important for local O_3 production. Figure 2 shows a record of the CARB estimated anthropogenic NOx and ROG and biogenic/natural ROG emissions for summer since 2000 for the South Coast air basin (CARB 2019). This analysis uses a base year of 2012 and projects forward from there. While the rate of emission decline has slowed, nonetheless, there is no suggestion in this inventory that the emissions have started to go back up. Figure 2 also shows weekday and weekend NOx emission for 2010 from a recent analysis for 2010 (Kim et al 2016).

The emissions reductions in the South Coast basins over the past several decades have clearly reduced O_3 concentrations but have also changed the photochemical environment. These changes include, for example, changes to the VOC/NOx emission ratios (Pollack et al 2013) and reducing the weekend/weekday differences (Baider et al 2015). At the same time climate change and meteorology also play important roles on O_3 production both in the short and long term (e.g. Pusede et al 2015; Jacob and Winner 2009). Horne and Dabdub (2017) model the impacts of climate change on O_3 in the south coast airshed and find a very significant increase in O_3 due to future temperature changes for the late 21^{st} century. A recently published study (Cai et al 2019) reported on results and modeling from the 2010 CalNex study. They reported lower NOx on weekends, with weekend/weekday emission ratios for NOx of ~0.75. This results in higher OH, HO_2 and O_3 on weekends, since NO_2 quickly reacts with OH to form HNO_3 and this

will suppress O_3 formation. They also report that while industrial VOCs are reasonably modeled, biogenic VOCs appear to be under-estimated.

In an alternate approach, Qian et al (2019) use an empirical method to derive O_3 isopleths and its sensitivity to ROG and NOx emissions for the South Coast airshed through 2016. These results indicate that the region is currently near the "ridge line" on the isopleths (the region of optimum ROG/NOx ratio for O_3 formation) and therefore the design value should be sensitive to both ROG and NOx emissions. However, this analysis is based purely on the anthropogenic emissions. We argue that the under-estimates in all VOCs and the fact that the biogenics are mostly emitted during the O_3 season and these are essentially, uncontrollable, means that we need to focus on NOx as a means to reduce O_3 exposure and the design values. Additionally, Qian et al (2019) state "We found high linear correlations between ODV and NOx and VOC emissions….". Their analysis focused on 1975-2016. However my analysis (described below) indicates that since about 2009, the relationship between the reported NOx emissions and ODV has weakened considerably.

While NOx emissions have declined about 45% since 2009, the O_3 design value has not significantly declined in that time frame (see Figure 3). If the trend in emissions is correct, it is surprising that O_3 is not decreasing more. In this case, other factors must be responsible. As the anthropogenic ROGs decrease, biogenic ROG emissions are becoming an increasingly important share of the total. Also, other anthropogenic sources of VOCs may be under-estimated (McDonald et al 2018). Using the reported CARB emission data gives ROG/NOx molar ratio of about 3.5, 4.1 and 5.5 for 2000, 2010 and 2018 respectively. Given the uncertainties, and likely under-estimates of ROGs, the ROG/NOx ratio is now probably very close to the optimum ratios for O_3 production e.g. 7-10, especially during the O_3 season (Ashok and Barrett 2016).

A key question for the South coast airsheds is whether NOx emissions are continuing to decline and, if so, how is this impacting O_3 formation. Silvern et al (2019) argue that the national decline in NOx emissions has continued through 2017, although the trend is slowing as industrial emissions are reduced and natural sources become a bigger part of the total. They also report that the relative changes in the tropospheric column of NO_2, measured by satellite borne Ozone Monitoring Instrument (OMI), shows smaller changes compared to surface observations. They

argue that this indicates an increasing role for non-urban sources (e.g. lightning, soils, etc) in the total tropospheric NO_2 column. In this report, I will examine the available evidence for NOx emission changes in the South coast using both surface and OMI data.

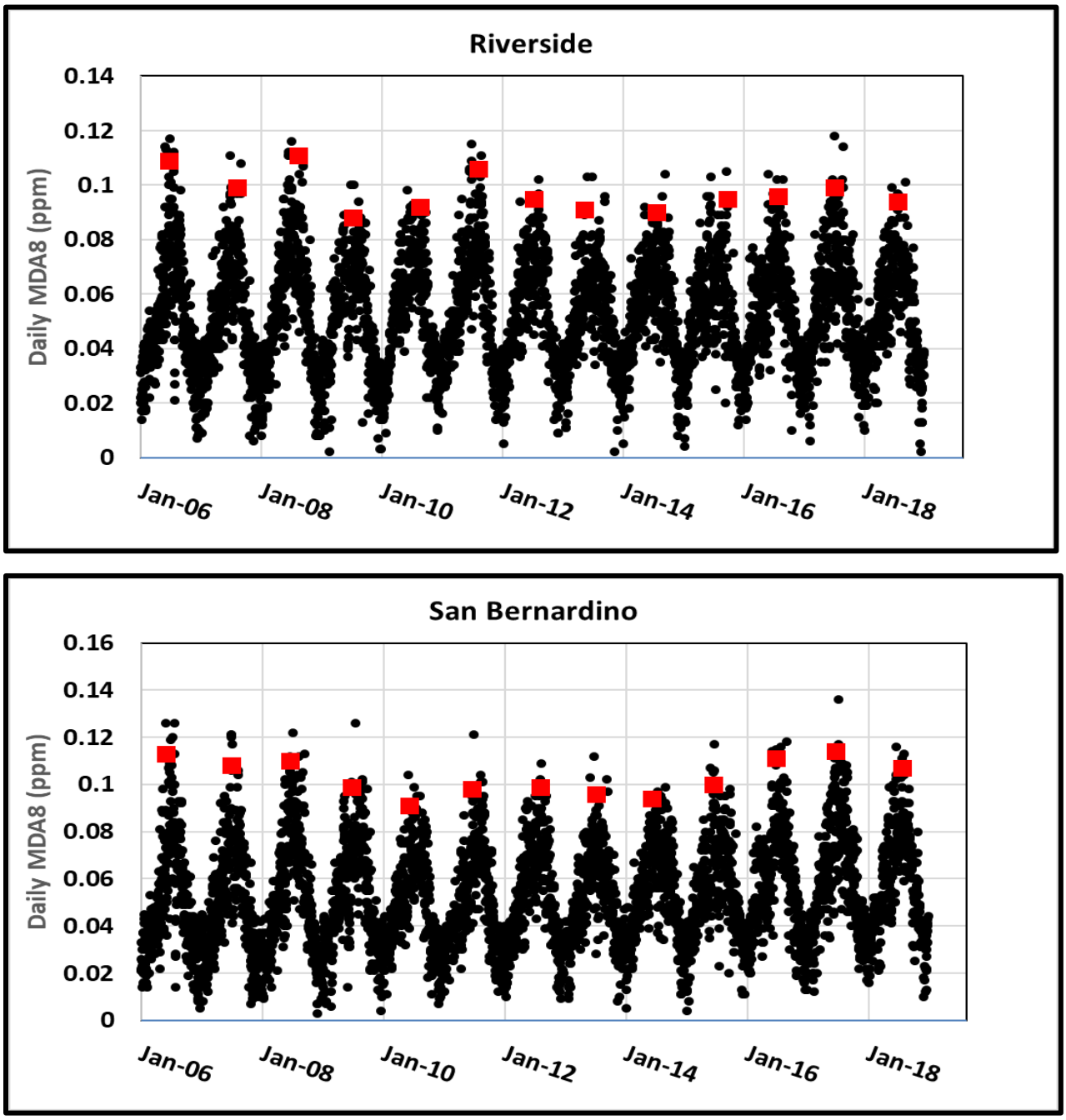

Figure 1. Daily MDA8 and annual 4th highest values for Riverside (top) and San Bernardino (bottom) monitoring sites (AQS 60658001 and 60719004, respectively) for 2006-2018. The 4th highest value each year is shown by the red square.

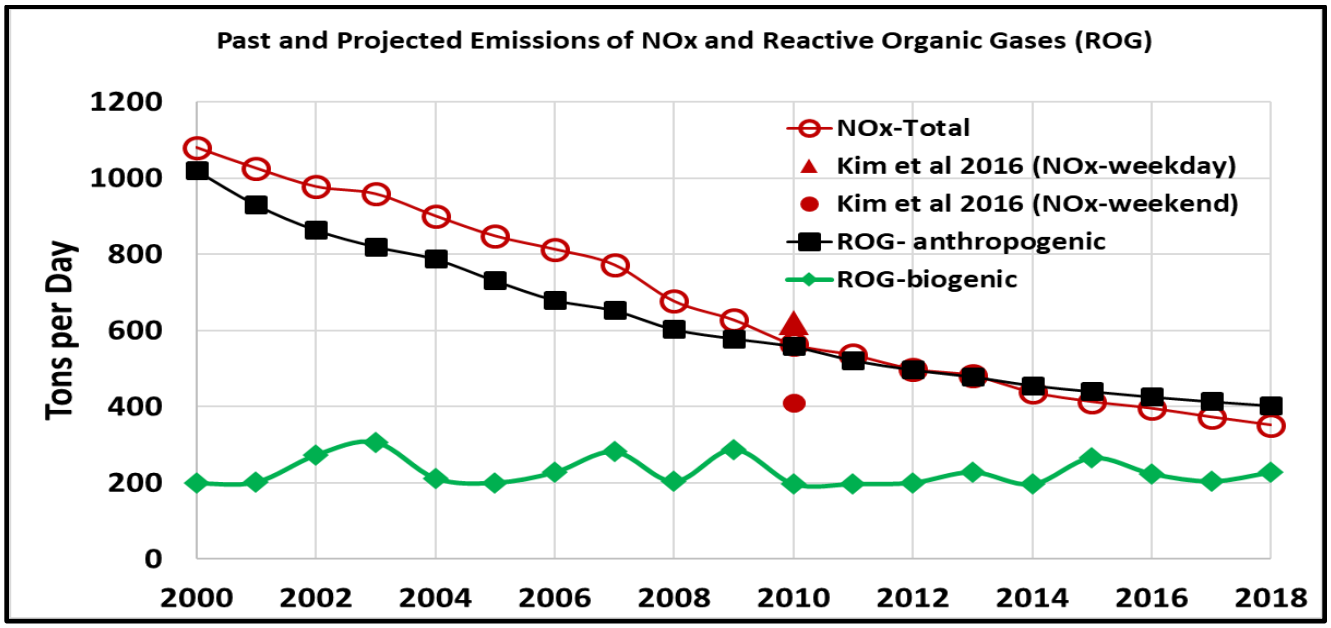

Figure 2. Daily emissions of NOx and ROGs for summer in the South Coast air basin. Data for 2000-2018 are from CARB (2019), with a base year of 2012. For ROG, these are separated according to anthropogenic (industrial plus mobile) and biogenic/natural emissions. Also shown are NOx emission estimates from Kim et al (2016) for both weekday and weekend days for the year 2010.

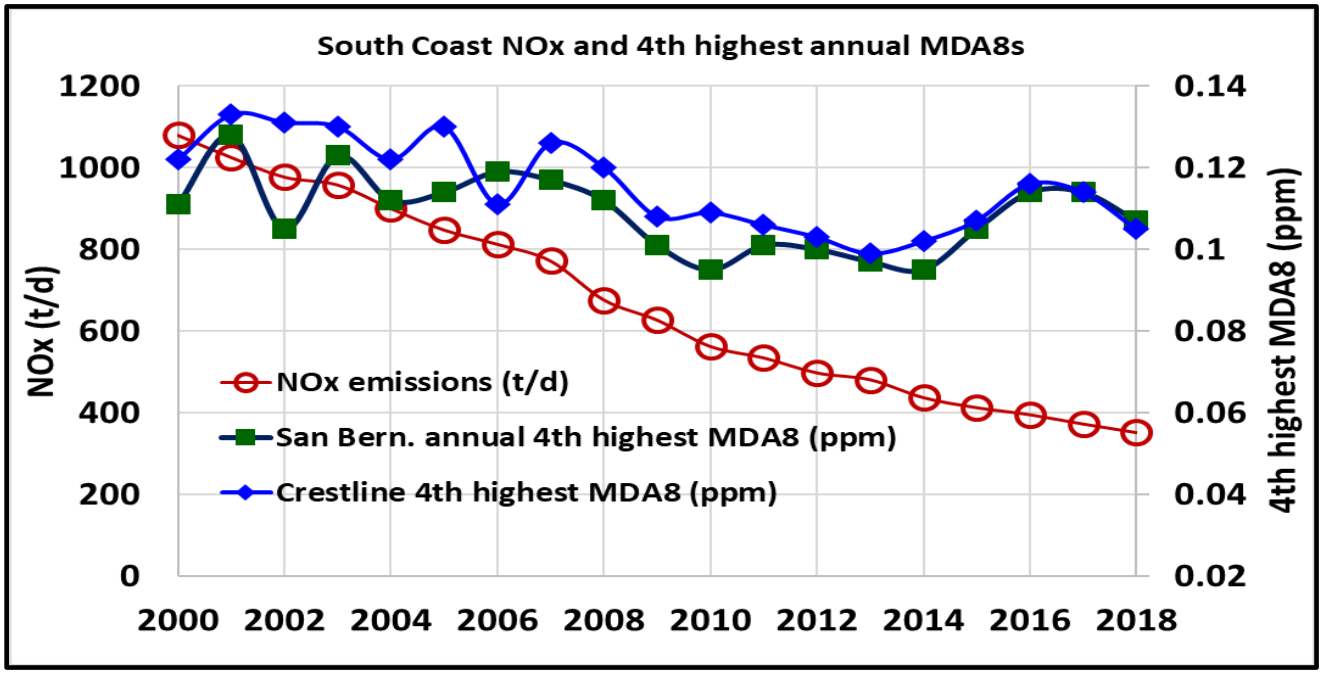

Figure 3. Daily emissions (summer) of NOx in the South Coast air basin and annual 4th highest MDA8 from the San Bernardino and Crestline monitoring sites. Emission data for 2000-2018 are from CARB (2019).

One aspect that is particularly difficult to model is O_3 production due to fire emissions (Jaffe et al 2012; 2018). This is especially relevant given the recent increase over the last decade in fires across the western U.S. (Dennison et al 2014; Westerling et al 2016; Abatzoglou et al 2016 ; McClure and Jaffe 2018; Laing and Jaffe 2019). Baker et al (2016; 2018) have shown that Eulerian models have great difficulty in correctly calculating the O_3 produced from fires. This is due to multiple factors including inadequate chemical mechanism, uncertainty in emissions, inadequate grid resolution and/or other factors.

We have previously used Generalized Additive Models (GAMs) to predict the MDA8 O_3 concentrations based on daily variations in meteorology (Gong et al 2017; 2018; McClure and Jaffe 2018; Jaffe et al 2018). GAMs are robust and flexible regression models that can incorporate linear and non-linear relationships, as well as categorical variables. Typical GAM results demonstrate an ability to predict MDA8 O_3 with an R^2 of between 0.6-0.85. This is a type of "machine learning" which uses a training dataset to understand the complex and inter-related patterns in the data. The difference between the GAM statistical prediction and the observed value is called the residual.

We have also used GAMs to quantify the additional O_3 associated with wildfire smoke influence. In these cases, we find that the residual is unbiased on non-smoke days, but has a significant positive bias on smoke influenced days. This bias is due to enhanced O_3 production on smoke influenced days, and can then be used to give an estimate of the O_3 produced from the fire emissions (Gong et al 2017; McClure et al 2018; Jaffe et al 2018). As part of our routine quality control measures, we also examine the predictions for non-smoke days that were not part of the original training dataset (cross validation). This same method can be used to identify patterns in the MDA8 associated with airmass trajectories, temperature, etc (Gong et 2017; 2018) and thus provides important information to understand the meteorological drivers for daily and inter-annual variations in O_3 or long term changes.

To identify smoke, we use the daily product from the NOAA Hazard Mapping System-Fire and Smoke Product (hereafter simply HMS). This product is based on analysis of multiple satellite products, both geostationary and polar orbiting. The HMS product is useful in our analysis as it is the only routine/daily data product to demonstrate overhead smoke at a given location.

Nonetheless, the frequency of smoke detection at any site is likely an under-estimate for various reasons (Kaulfus et al 2017; Buysse et al 2019). It is also important to recognize that the HMS data provide a view of overhead, not surface smoke. Thus, it is essential to combine the HMS product with surface $PM_{2.5}$ data to verify whether smoke is at the surface or not (e.g. Gong et al 2017).

2. Project goals

I. Examine relationships between MDA8 O_3 and key meteorological predictors, as well as satellite and surface observation of NO_2 for 2006-2018. Examine key relationships by year and day of week.

II. Develop a smoke classification for the South Coast airshed based on the HMS satellite product and surface $PM_{2.5}$ concentrations.

III. Develop GAM statistical models for five high O_3 sites plus one background site (Vandenberg AFB) in the South Coast airshed using meteorology and satellite observations as predictors that can characterize the maximum daily 8-hour average (MDA8) O_3 for 2006-2018. The GAMs will be developed using a training dataset consisting of 90% of the non-smoke day data, with 10% reserved for cross-validation (CV).

IV. Using the GAMs from the non-smoke training dataset, predict the expected O_3 for the smoke day dataset. This assumes that there is no impact from smoke on O_3 (null hypothesis). We can then use the GAM results to evaluate this hypothesis for each site.

V. Examine the long-term temperature changes in the south coast airshed in comparison to global patterns of temperature change and use this to examine the O_3 sensitivity to temperature. From this, I can estimate the significance of any recent temperature increases on O_3.

3. Methodology

3.1. Datasets used

A variety of datasets were used in this analysis (see Table 1). I carried out quality control on all datasets by removing missing data and obvious outliers, incorrect or unrealistic values. When possible, I compared similar variables from different sources. For example I compared daily temperature values from multiple observations and models to ensure that these are reasonably consistent. Note that not all datasets in Table 1 were actually used. Each dataset was examined and used, or not, depending on what was found.

Table 1. Air quality, meteorology and satellite datasets used in this analysis.

Ozone monitoring data (MDA8)

Site name	AQS ID	Coordinates, alt.	2016-2018 ODV	Source
San Bernardino (SBO)	60719004	34.11,-117.27, 316m	110 ppb	AQS-API
Riverside (RRO)	060658001	34.00,-117.42, 248m	94 ppb	AQS-API
Pomona POMO	060371701	34.07,-117.75, 279m	91 ppb	AQS-API
Glendora (GLO)	60370016	34.14,-117.85, 278m	103 ppb	AQS-API
Vandenberg AFB (VAFB)	060834003	34.60,-120.63,94 m	60 ppb	AQS-API
Crestline (CRO)	060710005	4.24,-117.27, 1387 m	110 ppb	AQS-API

NO_2 and $PM_{2.5}$ monitor data

Dataset	Locations	Source
Average daily max for all valid NO_2 data.	All monitors in Los Angeles and Riverside MSAs	EPA AIR Data
Daily mean for all valid $PM_{2.5}$ data.	All monitors in Los Angeles and Riverside MSAs	EPA AIR Data

Meteorological datasets

Dataset	Location	Source
Observed surface meteorology: T_{max}, T_{min}, daily average relative humidity (RH).	Surface observations from LAX and Riverside airports. For Riverside missing data are filled with mean of Riverside Fire Station and Citrus experimental station.	NOAA Climate Data Online
Radiosonde data products: 850 and 700 hPa temps, 0-1 km temperature, RH, wind speed and direction, WV mixing ratio. Parameters calculated from full sounding data: mixed layer mixing ratio, convective available potential energy (CAPE), lifted condensation level, mixed layer theta and thickness (1000 to 500 hPa).	Vandenberg AFB radiosondes. San Diego radiosondes.	University of Wyoming server
Point to point direction and distance from 12-hour back-trajectories	HYSPLIT model with GDAS 1ºx1º met dataset.	NOAA-Air Resources Lab
NASA Merra-2 assimilation/model, 2-meter min, max, mean temps,	LA Basin bounding box (West, South, East, North) 118.5º W, 33.5 º N, -117.5 º W, 34.5 º N	NASA Giovanni
Upper air products from North American Regional Reanalysis: surface RH and P, 2-meter min and max temps, geopotential heights at 500 and 700 hPa.	Grid cell centered at: 34.1ºN, 117.75º W	NOAA ESRL

Satellite data

Dataset	Locations	Source
NASA AIRS/Aqua satellite 700mb O_3 for both ascending (A) and descending (D) values	LA Basin bounding box (West, South, East, North) 118.5° W, 33.5 ° N, -117.5 ° W, 34.5 ° N	NASA Giovanni
NASA UV-index/OMI, Aura satellite	As above.	NASA Giovanni
NASA NO_2 Tropospheric column, 30% cloud screened/OMI, Aura satellite	As above.	NASA Giovanni
Daily NOAA-HMS Fire and Smoke Product (HMS-FSP) over the South coast airshed	Archive of HMS KMZ datafiles (2006-2018)	NOAA-NESDIS

3.2. Development of Generalized Additive Models for South Coast air basin

Generalized Additive Models (GAMs) are powerful regression models that can include linear, non-linear and categorical variables. GAMs are thus excellent tools to examine the complex nonlinearities of air pollution (Wood, 2006, Carslaw et al., 2007, Camalier et al. 2007). For this project I modeled the MDA8 O_3 for each monitoring site listed in Table 1. Each site was modeled separately using identical meteorological data for the region. The GAMs were computed in R software with the "mgcv" package.

The GAM equation can be written as:

$$\boldsymbol{g(\mu_i) = X_i\theta + f_1(x_{1i}) + f_2(x_{2i}) + f_3(x_{3i}) + \cdots + \varepsilon_i} \quad \textbf{(1)}$$

where *i* indicates the *ith* day's meteorological observation. $f_j(x)$ are smooth functions of the meteorological data. The element $g_(\mu_i)$ is the "link" function, which specifies the relationship between the linear formulation on the right side of equation and the response μ_i. $X_i\theta$ represents a categorical relationship for predictors not subject to non-linear transformations. For $f_j(x)$ non-linear cubic regression splines (CRS) are used to represent the relationship between ozone and each meteorological parameter. In equation 1 ε_i is the residual and it should be unbiased with respect to each predictor that is included in the model. The link function can use either a log or Gaussian distribution; both have been applied to the ozone analyses (Camalier et al 2007; Gong et al 2017; 2018). The smoothness of each CRS is controlled by the number of knots (k). Generally, the number of knots should be sufficiently large so as to adequately fit the observed relationship, but not so large as to yield unrealistic relationships. If the effective degrees of

freedom (EDF) approaches the number of knots, then the number of knots should be reduced. This would most likely occur when including variables with high P values. In our analysis we used k=10, consistent with earlier work (Gong et al 2017; 2018; McClure et al 2018) and none of the EDFs approached the number of knots. In some cases, a predictor variable may exhibit a changing relationship with the predictand as a function of a third variable, typically a time varying component. In this case we can use an interaction term that fits a 2-d spline to both variables.

We examined a large number of predictor variables for inclusion in the GAMS (see Table 1). Each predictor was evaluated based on the degree to which it had explanatory power for the MDA8 and the degree to which it improved the overall model fit, without overfitting. To evaluate this, I used the Akaike information criterion (AIC), as described by Wood (2006). Lower values of the AIC represent a superior model. Individual predictors were also evaluated using the approximate p-value as computed by the mgcv program. Correlation between meteorological variables is acceptable and nearly impossible to avoid. For example the daily maximum surface temperature and afternoon radiosonde temperature typically show a strong positive correlation. Inclusion of both variables in a GAM is acceptable and may improve the model performance, as each variable could potentially explain different aspects of the O_3 relationship. On the other hand, inclusion of essentially duplicate variables (e.g. daily max temperature from two nearby stations) is not likely to improve model performance. If two nearly identical variables are included, one variable will typically show a high p-value and the AIC will increase, compared to inclusion of just one of these. Ultimately the goal is to find the optimum combination of the fewest variables that can explain the greatest amount of variance in the predictand.

3.3. Model validation and quality control

There are several methods to examine the underlying assumptions of homogeneity, normality, and independence (Wood, 2006). To examine the quality of the model, we look at a number of factors, including:

1. The residuals (observed value minus fit value) should be normally distributed and not exhibit heteroscedasticity.
2. The residuals should not show bias with respect to any of the model predictors.
3. The cross-validation predictions should demonstrate similar skill at predictions as the training dataset and should have no bias with O_3 or any of the predictors.

We can use the gam.check code in R software to check the QQ plots (sample quantiles against theoretical quantiles), scatterplots (residuals against linear predictor), histogram of the residuals and scatter plots (response against fitted values). These results are shown in the appendix.

4. Results

4.1. Results overview

To address the key goals we start by further exploring the data to develop a better understanding of the high O_3 days in the South Coast airshed. Figure 4 shows the monthly distribution of days exceeding three MDA8 O_3 levels and Figure 5 shows the annual distribution since 2006 for the San Bernardino site. From this, we can see that the primary O_3 season is May-September, but the greatest likelihood of high O_3 in June-August. The overall number of days has changed rather little since 2006. There was a slight decline in the number of days between 2010-2015, but an uptick for 2016-2018.

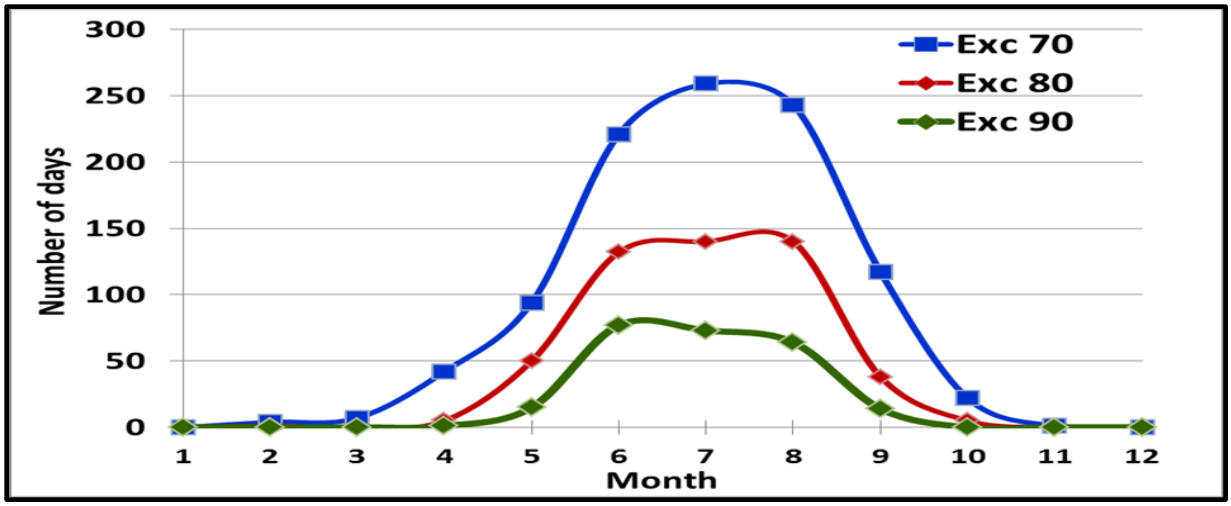

Figure 4. Cumulative number of days by month with MDA8 exceeding the given level (ppb) for 2006-2018 for San Bernardino site.

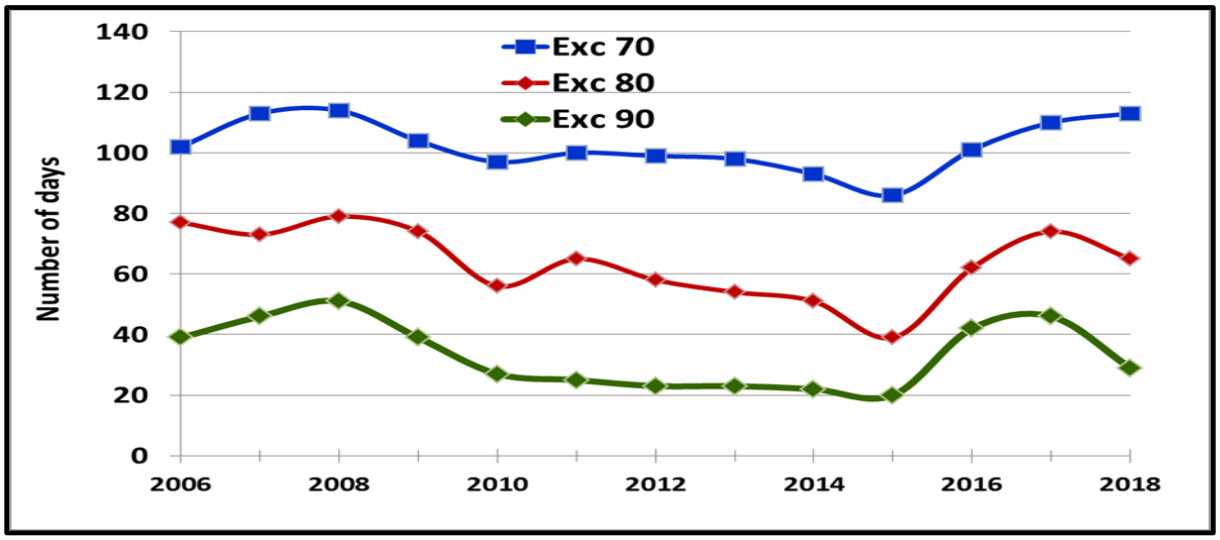

Figure 5. Cumulative number of days by year with MDA8 exceeding the given level for the San Bernardino site.

Figures 6 and 7 shows the weekly pattern of high O_3 days for the early and later periods for two O_3 levels and for the core O_3 season of June-August. The number of high O_3 days decreased on Sunday, went up significantly on weekdays and showed little change on Saturday. In the early part of this data record, weekday O_3 was clearly suppressed due to the reaction of O_3 with NO at high NOx concentrations. This weakening of the weekly cycle has been reported previously by Baidar et al (2015) and others.

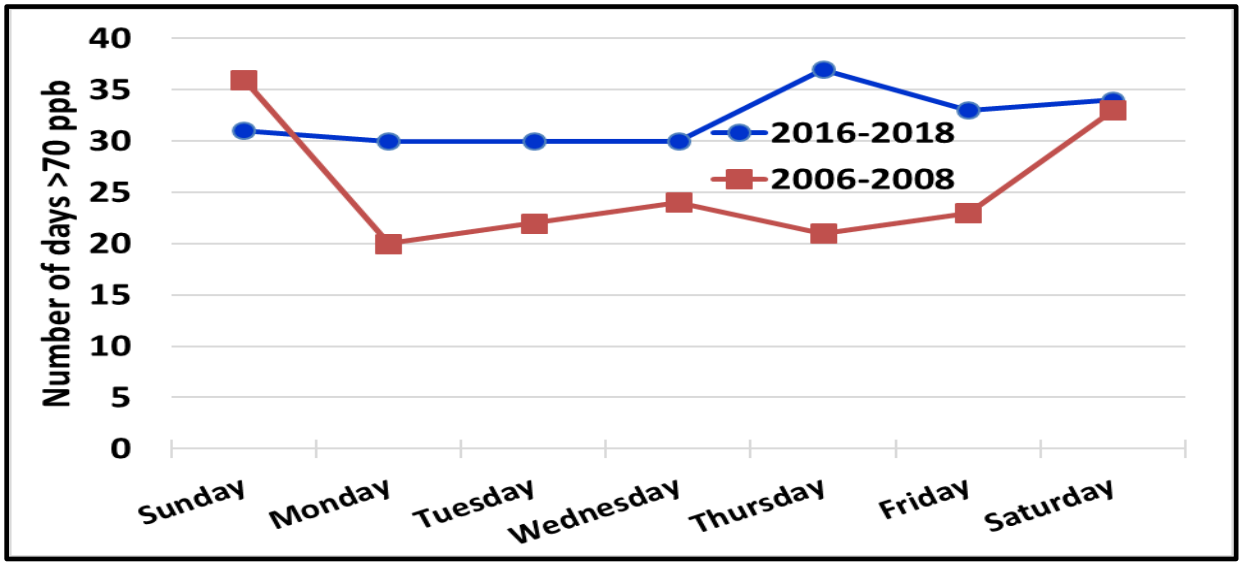

Figure 6. Number days with an MDA8 greater than 70 ppb for June-August, for San Bernardino site.

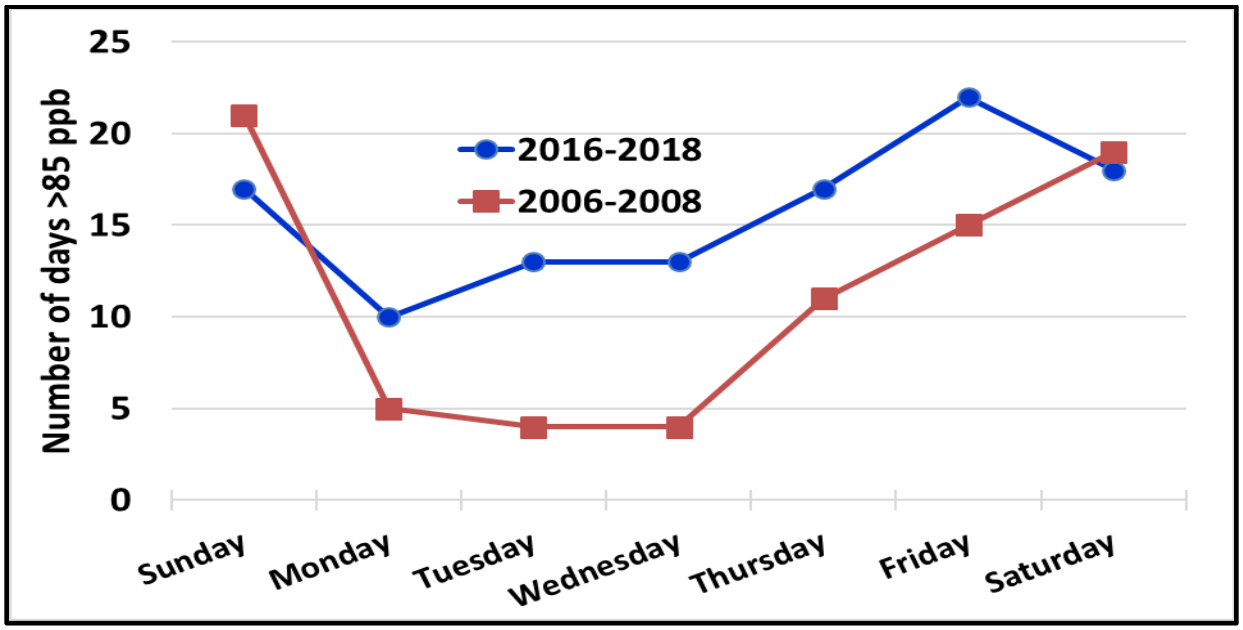

Figure 7. Number days with an MDA8 greater than 85 ppb for June-August, for San Bernardino site.

Figures 8 and 9 examine changes in NOx concentrations over the same time period, from surface monitors (Figure 8) and satellite (OMI) observations (Figure 9).

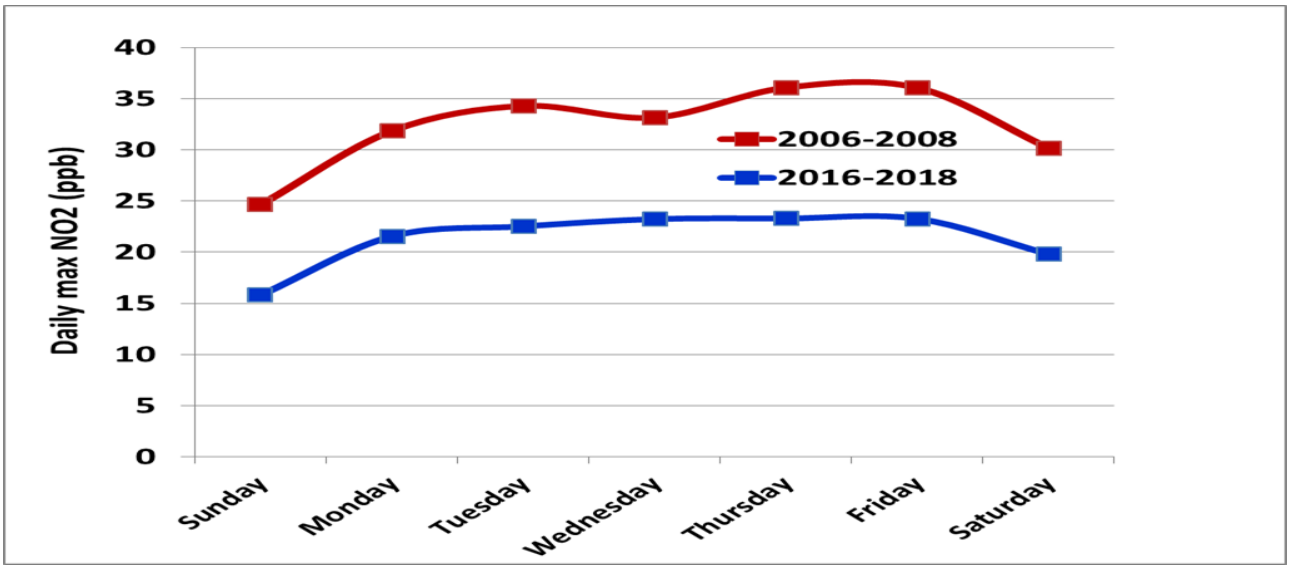

Figure 8. Average of Daily 1-hour maximum NO_2 (ppb) values for all Riverside area monitors by day of week for June-August.

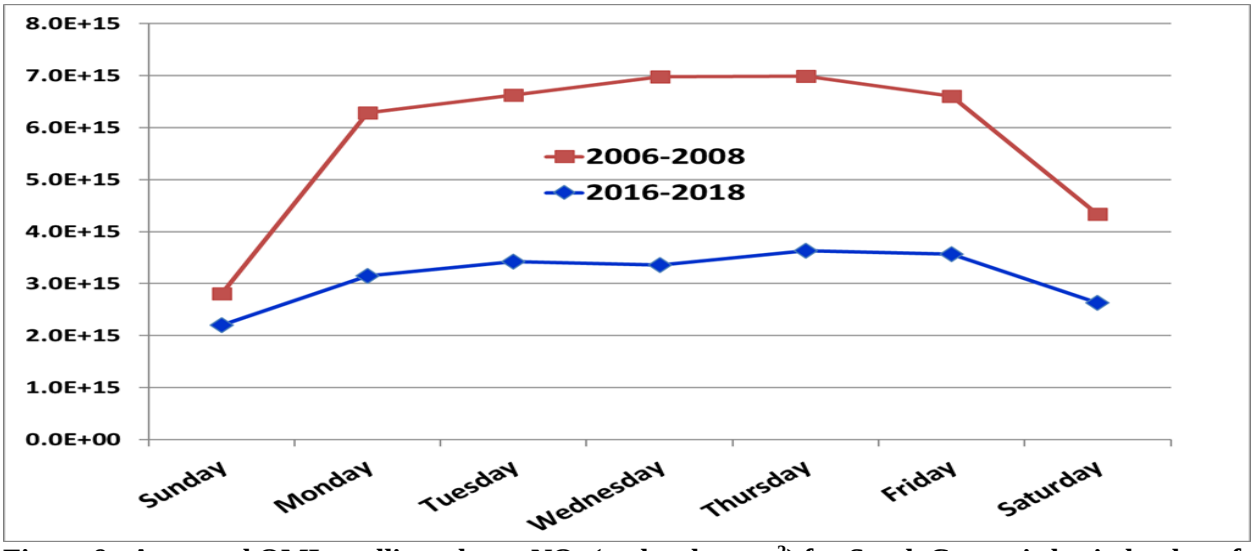

Figure 9. Averaged OMI satellite column NO_2 (molecules-cm^{-2}) for South Coast air basin by day of week for June-August.

Both the surface and satellite observations of NO_2 show a dramatic reduction in concentrations on all days, which is generally supportive of the reductions in emissions (e.g. Figures 2 and 3). Looking at Figure 8 in detail, we can see that current weekday NO_2 levels are similar to weekend levels for the earlier time period. This indicates that the increase in high O_3 days in the recent

time period is due to a reduction in NOx suppression of O_3. Its important to note that the observations show a reduction in the number of high O_3 days on Sunday, which is the day with the lowest NOx concentrations, as observed both by the surface monitors and satellite observations. This tells us that for Sunday, we have likely transitioned to a NOx limited regime. As NOx concentrations for all days start to reach the levels seen currently on Sundays, we would expect a rapid decrease in the number of high O_3 days, assuming VOCs also continue to decline slowly.

Next we examine the temporal trend in the reported NOx emission inventory (EI) vs observations. Figure 10 shows this comparison.

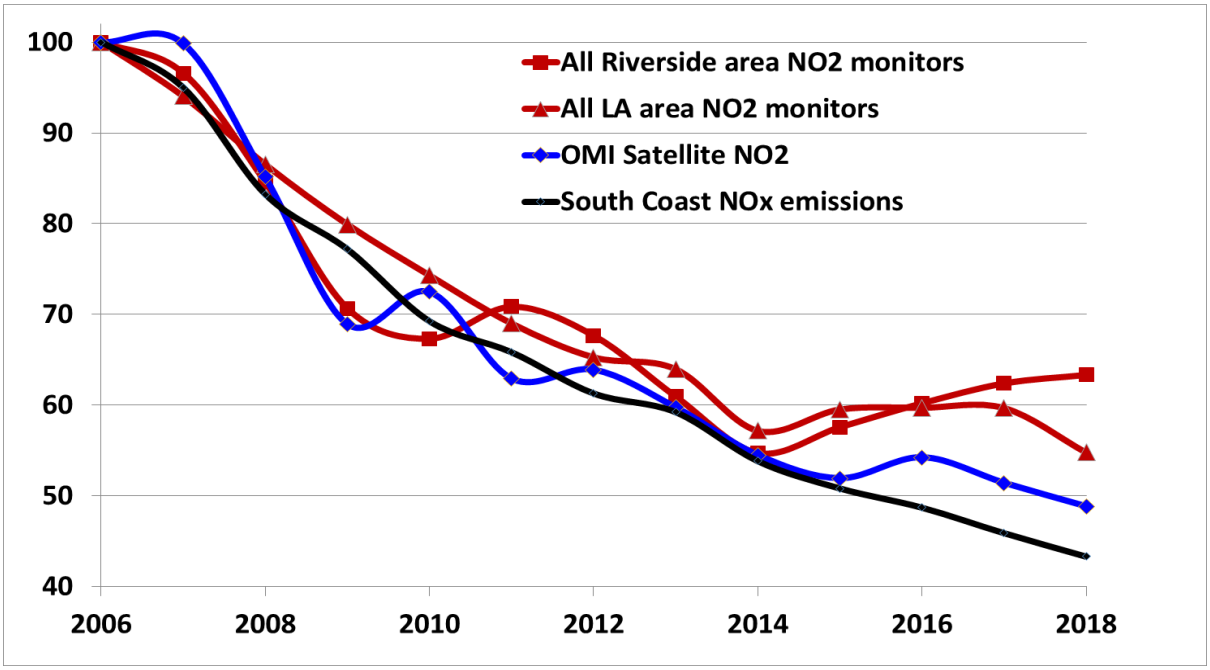

Figure 10. Different measures of south coast NOx for summer (June-August). All values are normalized to a 2006 value of 100.

All measures show a consistent reduction in NOx for 2006- 2014. However starting in 2015, the EI and observed NO_2 start to diverge. For the Riverside MSA there is a suggestion of flat or increasing NOx in the atmosphere. The OMI satellite observations show a similar pattern. Silvern et al (2019) argue that as U.S. NOx emissions decline, satellite observations of NO_2 may not follow monotonically, since at lower surface concentrations free tropospheric NO_2 starts to contribute a greater fraction of the total column. However this should be seen once the column density reaches much lower values, ca $1\text{-}2x10^{15}$ molecules cm^{-2}. The South Coast airshed remains well above these levels so this is not likely to a be significant confounder at this point. Note that Figure 10 shows average summer data from all available monitors in the Los Angeles and Riverside CBSAs. If instead we redo this analysis using only a core set of monitors with near continuous records from 2006-2018, we see a very similar result. This is shown in Figure

A1 in the appendix. I also examined the changes in NO_2 since 2014 at each individual monitor in the LA and Riverside MSAs. This is shown in Table A1 in the appendix. Between 2014-2015 and 2017-2018 NO_2 monitors in the LA MSA dropped an average of 6.6% for summer observations. In contrast, monitors in the Riverside MSA have, on average, changed by an insignificant amount (+0.1 %) over the same time period. Thus, our conclusion here is that the NOx concentrations have been essentially flat since 2014, in contrast to a reported reduction of ~20% in the emission inventory.

4.2. Identification of smoke days

To identify smoke days, we use a combination of the NOAA HMS-FSP (hereafter just HMS) and surface $PM_{2.5}$. I followed a similar procedure as we have used in our previous publications (Gong et al 2017; McClure et al 2018). For a day to be identified as having surface smoke it must have evidence for smoke in the HMS product and the daily average $PM_{2.5}$ must be greater than the mean + 1 SD of the non-smoke days. Tables 2 and 3 show a summary of this analysis for the Riverside and Crestline sites. The higher $PM_{2.5}$ values in the basin sites (e.g. Riverside) make it more difficult to identify smoke days using this criteria. Thus fewer smoke days are identified for the basin, compared to Crestline.

Table 2. $PM_{2.5}$ data for days with and without overhead HMS smoke using the Riverside $PM_{2.5}$ data. This classification will be used for the SBO, RRO, POMO, GLO and VAFB sites.

	Average PM2.5-no HMS smoke (µg/m^3)	SD (µg/m^3)	N	Mean+SD (µg/m^3)	N smoke days	Average PM2.5 on smoke days (µg/m^3)
2006	19.27	12.17	272	31.45		
2007	18.95	12.13	253	31.08		
2008	16.28	9.22	315	25.50	3	29.43
2009	14.95	8.87	305	23.82	1	29.10
2010	13.19	7.35	339	20.54		
2011	13.82	7.97	355	21.79		
2012	13.72	7.11	352	20.82	1	21.10
2013	12.84	7.77	337	20.61	1	32.90
2014	15.74	7.23	345	22.97		
2015	11.76	7.34	336	19.10		
2016	12.28	6.87	331	19.16	1	23.60
2017	12.13	6.93	341	19.05	2	20.20
2018	11.99	6.63	305	18.62	4	18.95

Table 3. $PM_{2.5}$ data for days with and without overhead HMS smoke using the Crestline $PM_{2.5}$ data, which starts in 2009. This classification scheme will be used for the Crestline site.

	Average PM2.5-no HMS smoke ($\mu g/m^3$)	SD ($\mu g/m^3$)	N	Mean+SD ($\mu g/m^3$)	N smoke days	Average PM2.5 on smoke days ($\mu g/m^3$)
2009	10.98	4.87	137	15.84	7	28.50
2010	12.31	4.61	325	16.92	1	18.80
2011	13.08	5.23	236	18.31		
2012	9.10	4.29	352	13.38	3	17.30
2013	7.89	4.06	331	11.94	1	12.20
2014	9.40	4.35	349	13.75		
2015	7.91	3.93	313	11.84		
2016	6.38	4.01	320	10.39	13	16.24
2017	11.22	3.66	267	14.87	3	17.00
2018	8.94	3.44	302	12.38	13	16.46

4.3. GAM modeling results

The GAM models were developed for each site using the procedure described in Section 3.2. Because our focus is on the primary O_3 season, the GAMs were computed on the MDA8 data from May-September for 2006-2018. Each predictor variable used a single value each day and each O_3 monitoring site listed in Table 1 is treated separately. The dataset was split as shown in Table 4.

Table 4. Dataset selection process for GAMs.

Dataset	How chosen?	How used?
Training dataset	90% of non-smoke days, randomly selected.	This dataset was the basis for the GAM development at each site.
Cross-validation (CV) dataset	10% of non-smoke days, randomly selected.	This dataset was not part of the model development, but was used to independently evaluate the GAM predictions.
Smoke days	Selected as described in 4.2 above.	This dataset was not part of the model development, but was used to evaluate possible enhanced O_3 due to the presence of smoke.

I evaluated many different model formulations. Based on the available data and the criteria selection (described in section 3.2), I came up with two different GAM formulations one for the

lower elevation sites, including San Bernardino, Riverside, Pomona, Glendale, Vandenberg AFB and a second equation for the higher elevation Crestline site, which responded to a slightly different set of predictor variables. The equations for each are given below with an explanation of the variables in Table 5

Final GAM equation for basin sites (San Bernardino, Riverside, Pomona, Glendale, Vandenberg AFB):

Model_1 =
gam(SBO~s(TrDIST12,by=TrQ12)+s(Y,DOW)+s(Y,RivNO2)+s(UV,bs="cr",k=10)+s(T850M,bs="cr",k=10)+s(T850A,bs="cr",k=10)+s(RIVTMAX,bs="cr",k=10)+s(DOY,bs="cr",k=10)+s(THCKA,bs="cr",k=10)+DOW,data=dat3,na.action=na.exclude)

Final GAM equation for Crestline:

Model_2 =
gam(CRO~s(TrDIST12,by=TrQ12)+s(Y,DOW)+s(Y,RivNO2)+s(T700A,bs="cr",k=10)+s(UV,bs="cr",k=10)+s(T850M,bs="cr",k=10)+s(T850A,bs="cr",k=10)+s(RIVTMAX,bs="cr",k=10)+s(DOY,bs="cr",k=10)+s(THCKA,bs="cr",k=10)+s(MerTMAX,bs="cr",k=10)+DOW,data=dat3,na.action=na.exclude)

Table 5. Variables used in GAM equations.

TrDIST12: 12 hour point to point back-trajectory distance (km)
TrQ12: 12 hour point to point back-trajectory quadrant (e.g. NE, SE, SW, NW)
DOW: day of week
Y: year
RivNO2: Average of all Riverside surface NO_2 monitors
UV: satellite measured (OMI) UV index
T850M: 850 hPa temperature from San Diego morning sounding.
T850A: 850 hPa temperature from San Diego afternoon sounding.
T700A: 700 hPa temperature from San Diego afternoon sounding.
RivTMAX: Observed daily maximum temperature observed at the Riverside airport.
DOY: day of year.
THICKA: 1000 to 500 hPa from afternoon San Diego radiosonde.
MerTMAX: Two-meter daily maximum temperature from NASA Merra-2 model
DOW: day of week.

Terms listed with an s are fit via non-linear splines. Terms listed with a "+" (e.g. DOW) are treated as non-numeric categorical variables. Interaction terms are shown as "s(Y,DOW)", which indicates the 2-d spline fits mentioned earlier. Terms listed with "by" indicate the splines should be computed independently for each separate category of the variable. In other words the term "s(TrDIST12,by=TrQ12)" indicates that the splines should be computed for each category of the trajectory quadrants independently.

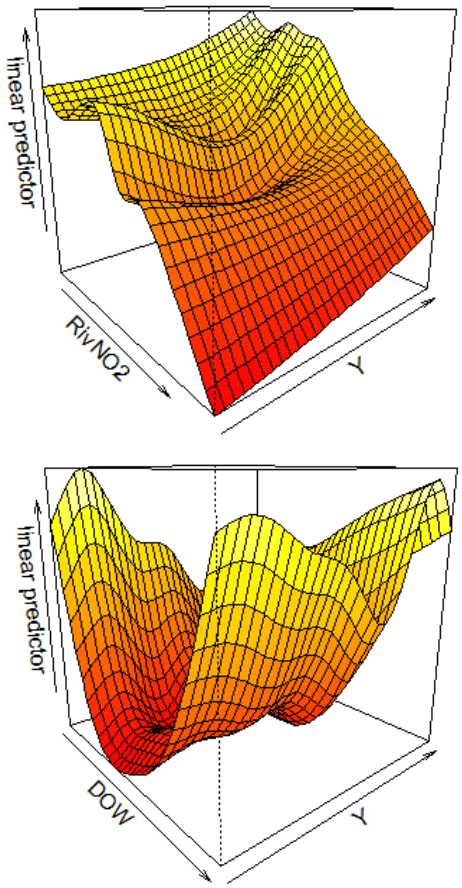

Figure 11a,b. 3-d plot showing the spline fit to Riverside NO_2 by year (11a, top) and Day of week (DOW) by Year (11b, bottom), both for the San Bernardino MDA8 values. The "linear predictor", on the Z-axis, indicates the contribution of each variable to the MDA8 O_3. The X and Y axis arrows indicate the direction for increasing NO_2, DOW (starting with Sunday) and Year.

Because of the changing relationship between O_3 and NO_2 and day of week, it is difficult to capture this effect in a standard GAM spline fit, which only considers one variable at a time. Including variable interaction terms lead to significantly improved results. Figures 11a,b show examples of the results of the interaction terms. Figure 11a shows that at the highest NO_2 values, O_3 is generally suppressed across all years. Figure 11b shows the O_3 suppression is greatest in midweek, and this is most pronounced in the early part of the data record.

Given the optimum equation, we can now move to the full GAM results. Table 6 shows a summary of the GAM results for each O_3 monitoring site and split by the three datasets described in Table 4.

Table 6. Summary results for the Generalized Additive Modeling for 6 sites in the South Coast air basin. Results for the training dataset are in black, the cross-validation dataset is in blue and the smoke dataset is in red. The last line in each grouping states whether the residual is significantly different from zero at a 95% confidence interval.

	SBO	RRO	POMO	GLO	VAFB	CRO
Count of training days	1462	1462	1462	1462	1462	1438
Mean obs MDA8 training (ppb)	70.19	68.18	59.00	63.18	36.13	75.75
Mean RivTMAX training (ºF)	89.93	89.93	89.93	89.93	89.93	89.81
R^2 training	0.76	0.70	0.67	0.72	0.53	0.70
Mean residual	-4.3E-12	-2.0E-11	-4.6E-11	9.7E-13	-8.9E-13	-6.4E-13
SD residual	8.59	8.14	8.52	8.71	5.75	9.72
95% C.I.	0.44	0.42	0.44	0.45	0.30	0.50
Resid sig diff from zero?	No	No	No	No	No	No
Count of cross validation days	160	160	160	160	160	157
Mean obs MDA8 CV (ppb)	71.05	68.76	59.58	64.34	36.25	75.60
Mean RivTMAX CV (ºF)	90.15	90.15	90.15	90.15	90.15	89.99
R^2 Cross validation	0.69	0.66	0.61	0.67	0.47	0.65
Mean residual	0.21	0.16	0.22	0.31	-0.11	-0.68
SD residual	9.40	8.45	8.44	9.03	6.77	10.36
95% C.I.	1.47	1.32	1.32	1.41	1.06	1.63
Resid sig diff from zero?	No	No	No	No	No	No
Count of smoke days	12	12	12	12	12	36
Mean obs MDA8 smoke (ppb)	83.15	76.15	70.31	78.92	32.82	90.78
Mean RivTMAX smoke (ºF)	95.96	95.96	95.96	95.96	95.96	97.78
R^2 smoke	0.57	0.42	0.63	0.78	0.35	0.45
Mean residual	1.92	0.27	4.28	3.42	-1.39	5.62
SD residual	11.44	12.50	15.08	12.53	5.75	10.88
95% C.I.	7.27	7.94	9.58	7.96	3.65	3.68
Resid sig diff from zero?	No	No	No	No	No	Yes

Figures 12-15 show example scatterplots for the observed vs GAM predicted MDA8s, both for the training dataset and CV for two sites (San Bernardino and Crestline). All of the urban, high O_3 sites show excellent predictability from the GAMs, with R^2 values of 0.67 to 0.76. The VAFB site shows worse performance, compared to the others sites (R^2 of 0.53). This is not a surprising result and is consistent with our earlier results (Gong et al 2017). Generally, the meteorological parameters are good predictors for local O_3 production but not as good predictors for large scale, transported O_3. This, combined with the fact that the range in MDA8 values is lower, leads to lower values of the R^2.

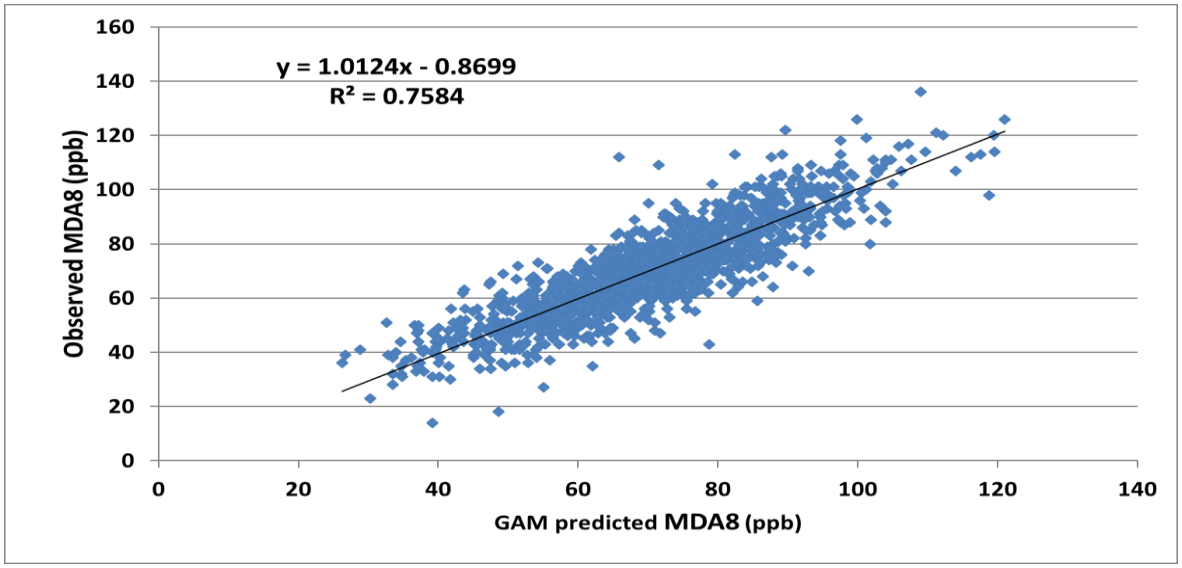

Figure 12. Observed and GAM predictions for the San Bernardino monitoring site from training dataset.

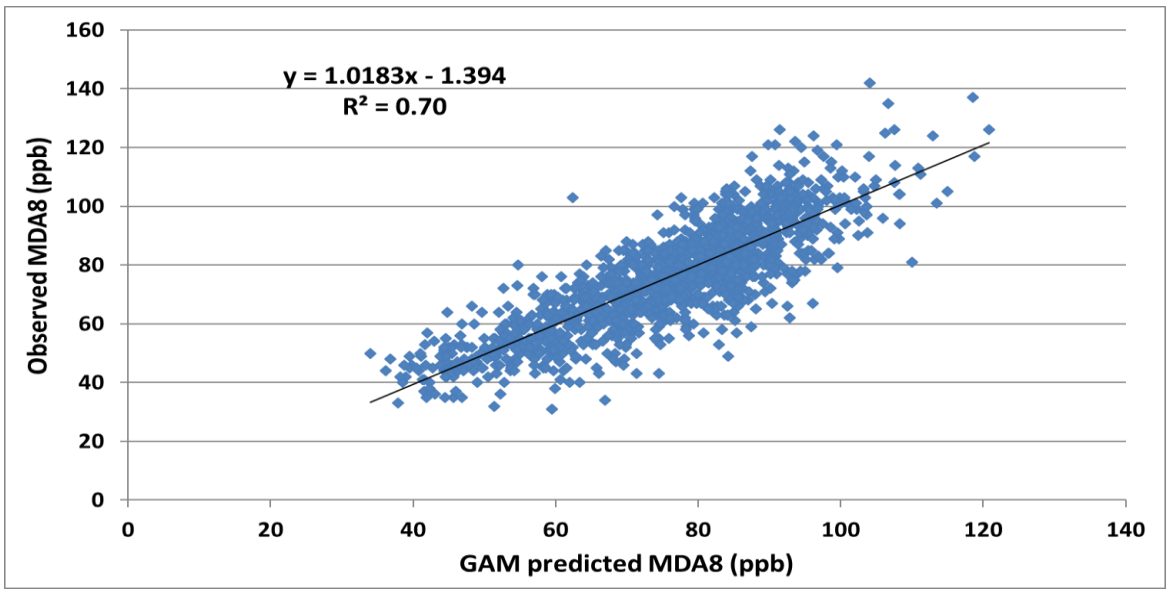

Figure 13. Observed and GAM predictions for the Crestline monitoring site from training dataset.

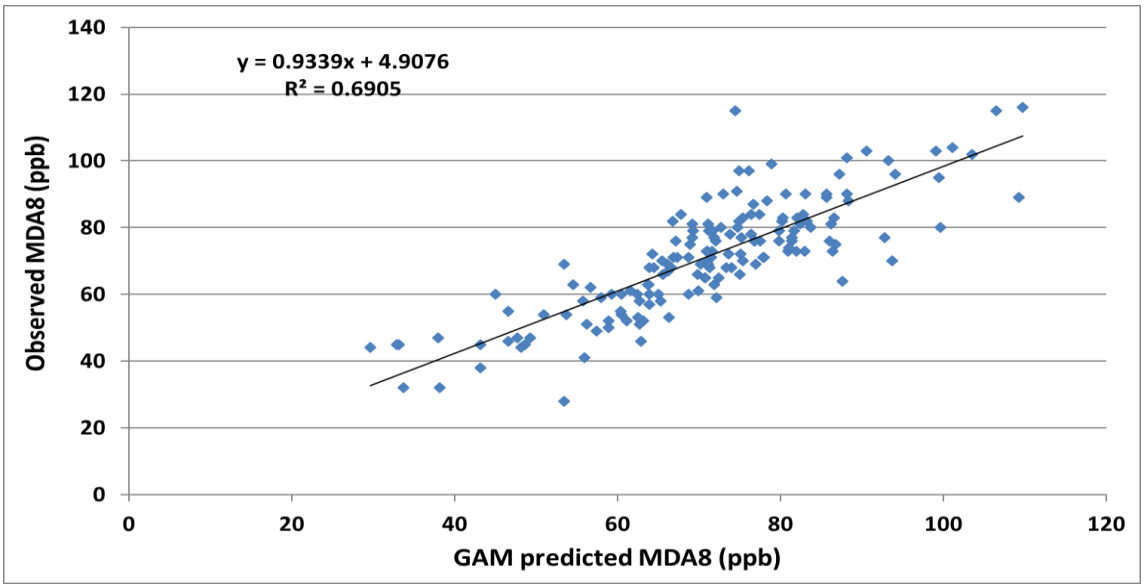

Figure 14. Observed and GAM predictions for the San Bernardino monitoring site from CV dataset.

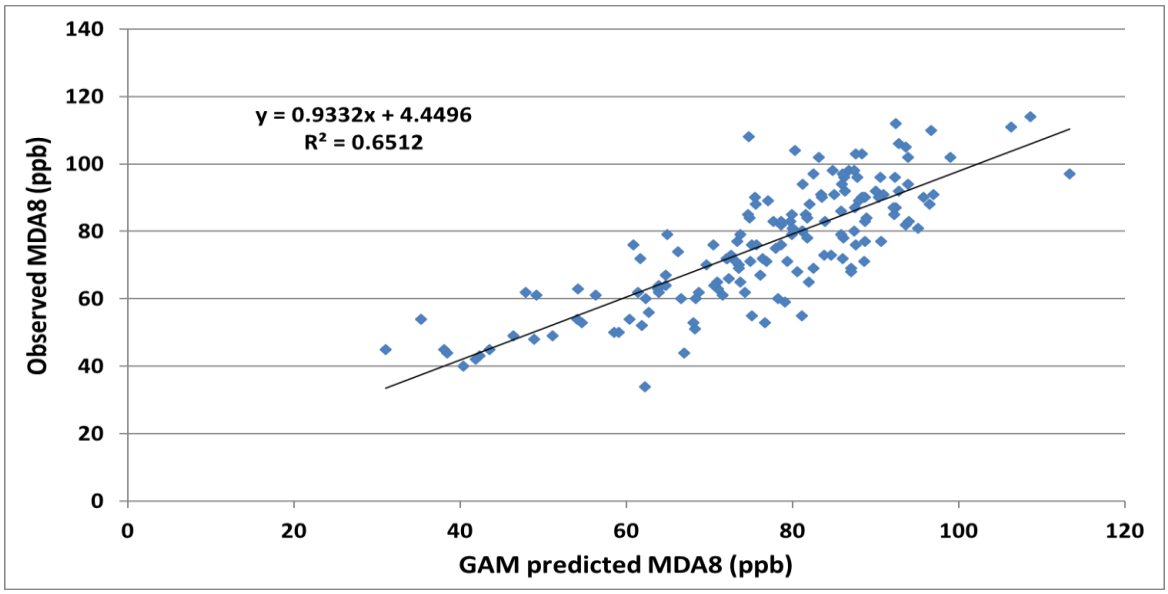

Figure 15. Observed and GAM predictions for the Crestline monitoring site from CV dataset.

4.4 Influence of smoke on O_3 MDA8s

Turning our attention to the smoke day results, we find that most sites in the SC basin do not show a significantly enhanced residual on the smoke days. This reflects the small number of smoke days, the small mean value and the large variability of the residuals. This is in contrast to our previous analyses for sites across the Western U.S. (Gong et al 2017; McClure et al 2018; Jaffe et al 2018). Only Crestline shows a significant enhancement in the residual on smoke days, with a mean enhancement of 5.6 ppb. Figures 16 and 17 shows the residuals for the training dataset and smoke days for San Bernardino and Crestline sites.

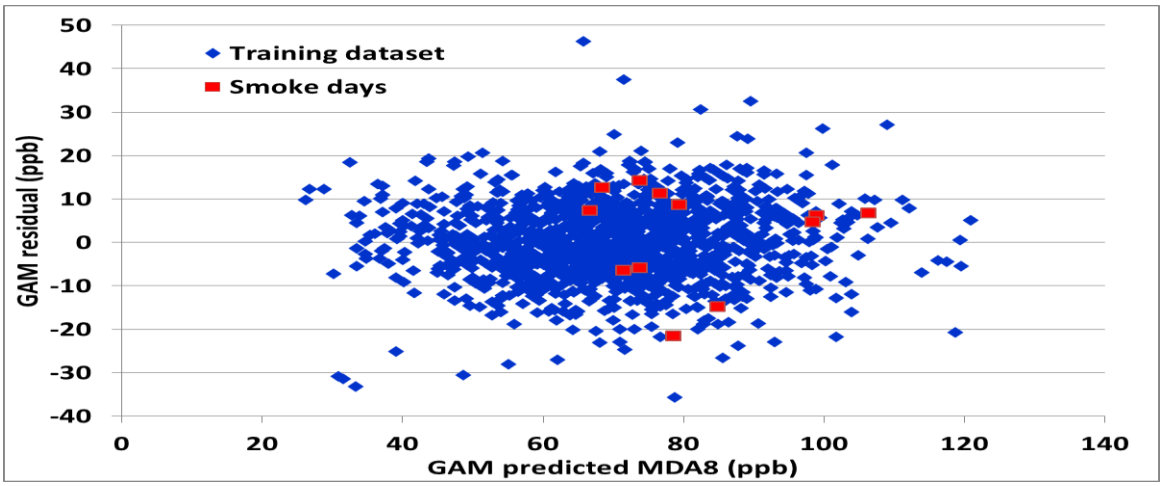

Figure 16. GAM residuals vs predicted MDA8 for the San Bernardino monitoring site. Blue points show results for the training dataset (n=1462), red points show results for the smoke dataset (n=12). The mean residual for the smoke dataset is 1.9 ppb, which is not significantly different from zero at a 95% confidence (see Table 6).

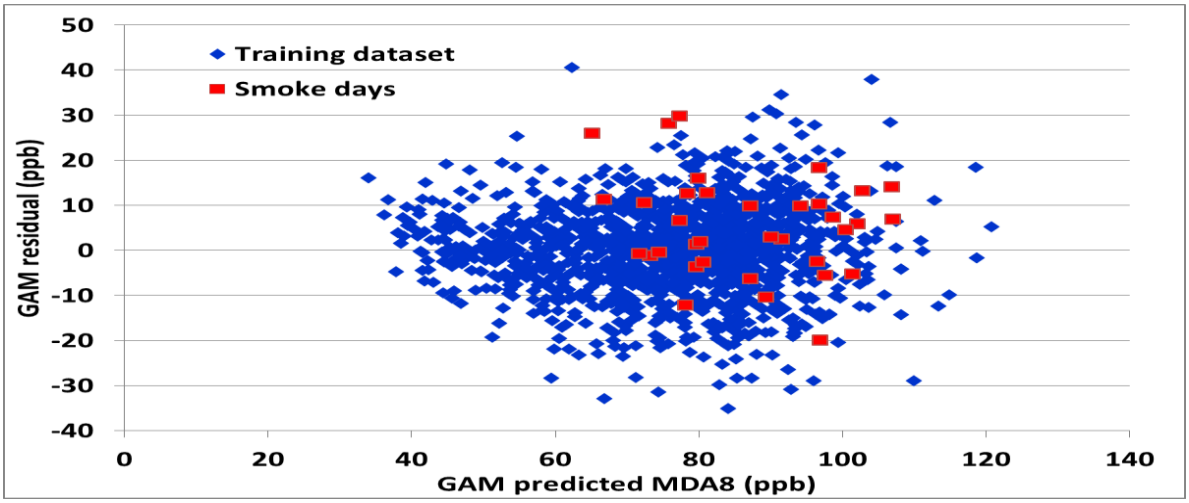

Figure 17. GAM residuals vs predicted MDA8 for the Crestline monitoring site. Blue points show results for the training dataset (n=1438), red points show results for the smoke dataset (n=36). The mean residual for the smoke dataset is 5.6 ppb, which is significantly different from zero at a 95% confidence (see Table 6).

Table 6 also shows that the mean O_3 at most sites and the Riverside Tmax for the training and CV datasets are nearly identical, but that smoke days have more O_3 and are significantly warmer. Given that the MDA8 goes up about 1 to 2 ppb for every 1^{o}F rise in the daily max temperature, as discussed in section 4.5 below and Table 9, the increased MDA8 on the smoke days can mostly be accounted for by the increase in temperature, except for Crestline. Here the increased MDA8 on smoke days (ca 15 ppb) is not fully accounted for by the increase in temperature and some of this increase must be associated with O_3, or O_3 precursors, associated with the smoke. Because temperature is included as one of the GAM predictors, and in fact one of the strongest predictors, the GAM residual should take into account the enhanced temperatures. Thus, we can expect that the enhanced residuals are due to the smoke influence alone.

Given the significant influence of smoke at Crestline, we can explore how important this is for the 2016-2018 design value calculation. Table 3 shows that there were 41 identified smoke days at Crestline for 2006-2018, 29 of which were in 2016-2018. Table 7 shows the impact on the annual fourth highest MDA8 for Crestline with and without all identified smoke days. This analysis shows that even if every single smoke day were eliminated from consideration, the 2016-2018 design value for Crestline would only change from 111 to 108 ppb.

Table 7. Annual fourth highest daily MDA8 for the Crestline with all data and with smoke days excluded. Note that the ODV is calculated by averaging the fourth highest value from the three previous years and truncating the result to 3 figures.

	Fourth highest observed MDA8 (ppb)	**Fourth highest observed MDA8 (if all smoke days excluded)**
2006	111	111
2007	126	126
2008	120	120
2009	108	108
2010	109	109
2011	106	106
2012	103	103
2013	99	99
2014	102	102
2015	107	107
2016	116	110
2017	114	114
2018	105	102
2016-2018 average	**111.7**	**108.7**
Estimated 2016-2018 ODV	**111**	**108**

4.5 Influence of climate change on O_3 MDA8s

Since smoke is not implicated in explaining recent high MDA8 values in the South coast airshed, we now turn our attention to the role of climate change. This is particularly important given the fact that daily max temperature (DMT) is an important driver for high O_3 days. For this analysis, I used two primary databases, the observed Riverside daily max temperature and the NASA MERRA-2 assimilation (for more information, see Gelaro R., et al., 2017, or https://gmao.gsfc.nasa.gov/reanalysis/MERRA-2/docs/). In short, MERRA-2 is a state-of-the-art weather/climate reanalysis at 0.5^o x 0.625^o resolution that incorporates a large number of observed and modeled products into a physically consistent representation of the atmosphere. MERRA-2 is available starting in 1980 and continues thru the present on an hourly timescale. For this analysis, I focus on the daily maximum temperature for 1980-2018, as reported by the Riverside met station and Merra-2 for a 1^o x 1^o grid cell centered at 118.0W, 34.0N. Figures 18 compares the two datasets for all days, but since much of this agreement is due to the seasonal cycle in temperature, a more useful comparison is done by only looking at summer days. So Figure 19 compares the two datasets for June-August. The comparisons show that the datasets have excellent agreement. There is a tendency for the DMT in MERRA-2 to be slightly cooler than the observations. This mainly reflects the broader coverage for MERRA-2(e.g. a 1^o x 1^o grid cell), compared to the point measurement at Riverside. This difference is not important for my analysis and, as noted previously, both datasets are strong predictors for the MDA8 in the south coast airshed.

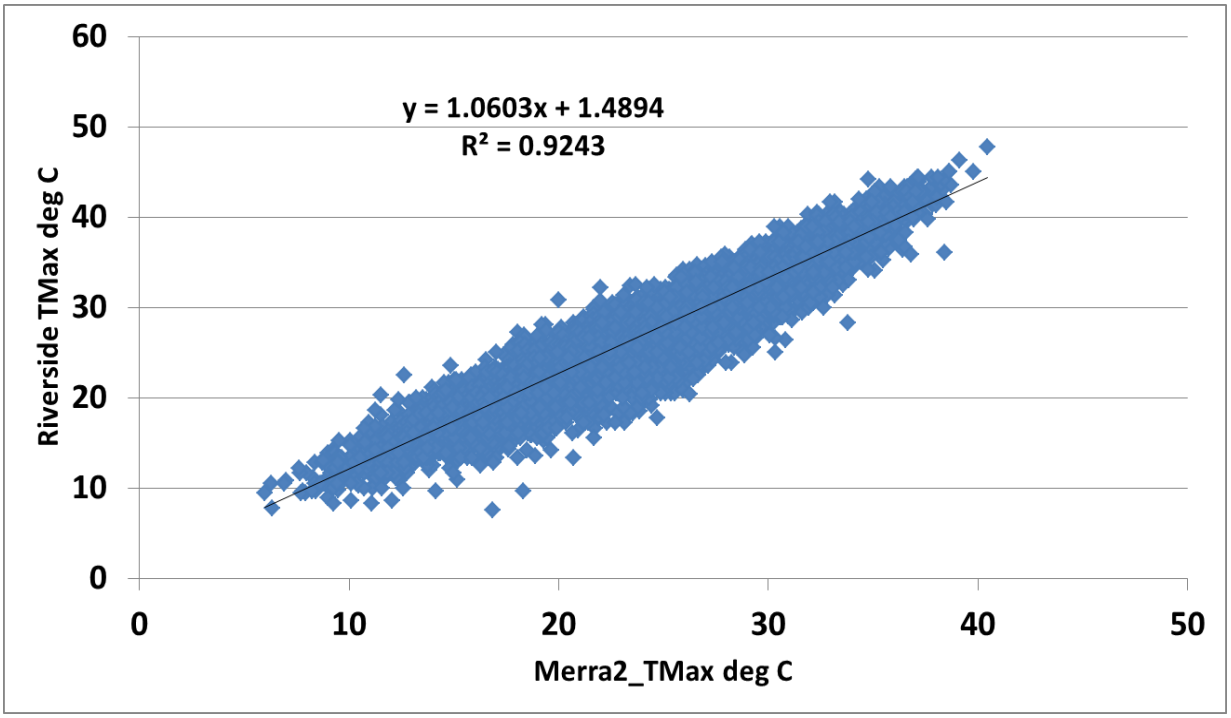

Figure 18. Scatter plot of Riverside daily Tmax vs Merra-2 Tmax for all days, 1980-2018.

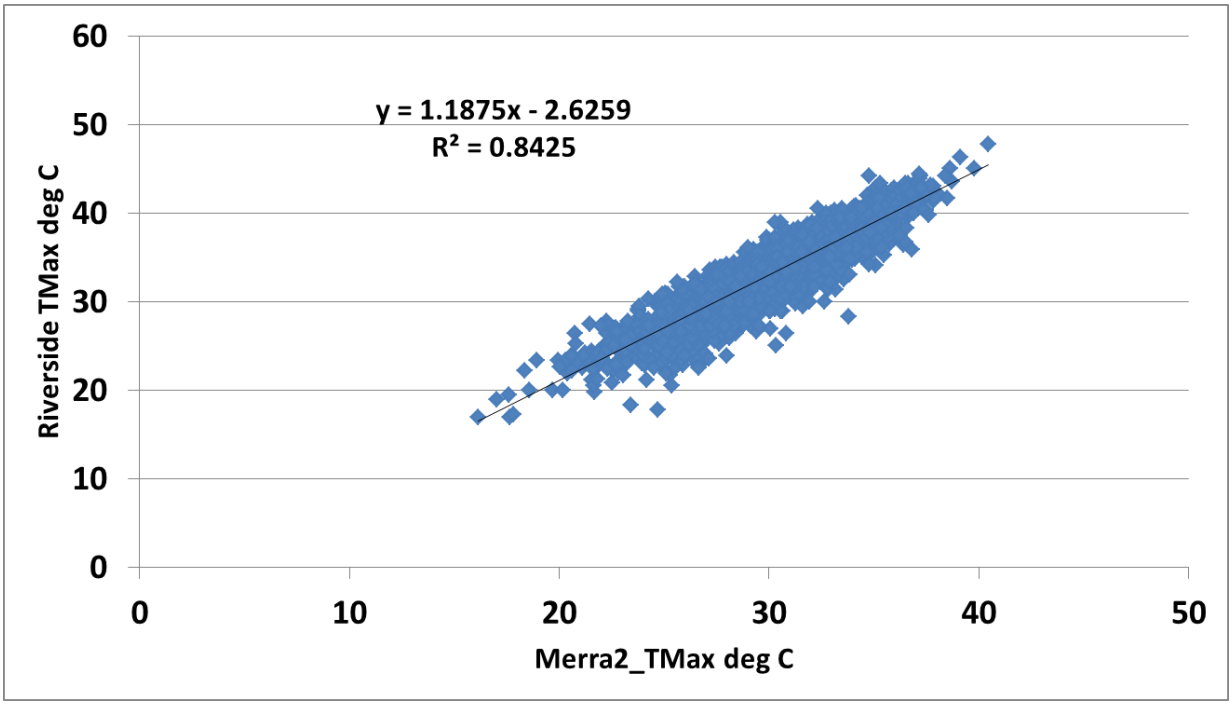

Figure 19. Scatter plot of Riverside daily Tmax vs Merra-2 Tmax for June-August days, 1980-2018.

Next, I look at temperature trends in the two datasets. Table 8 gives the annual and decadal average summer DMT for 1980-2018. While there is a large degree of year-to-year variations, the effect from global warming is evident, with the MERRA-2 analysis increasing by ~0.3ºC and Riverside values increasing by ~0.7ºC, over this time period. Figure 20 plots the annual average DMT for both datasets for June-September. There is a good correlation in the annual summer means between the two datasets ($R^2 = 0.68$). Both datasets show an increasing temperatures, 0.026 and .014 ºC/year for Riverside and MERRA-2, respectively, but only the Riverside data show a statistically significant increase. For reference, the most widely accepted global temperature records have been reported by NASA-Goddard Institute of Space Studies (GISS). The NASA-GISS global land-ocean temperature analysis shows an average increase of 0.02ºC per year since 1980, so the trend values for the south coast airshed are in-line with the increase in global mean temperatures.

Table 8. Annual summer (June-September) average daily max temperature (ºC) from the Riverside and NASA Merra-2 datasets.

Year	Merra2_Tmax	Riverside_Tmax		Merra2_Tmax	Riverside_Tmax
1980	29.8	33.1			
1981	32.0	34.6			
1982	29.1	30.9			
1983	29.5	32.7			
1984	31.6	34.0			
1985	30.7	33.7			
1986	29.6	32.8			
1987	29.9	31.9			
1988	30.3	32.6	10 year mean		
1989	30.3	32.9	1980-1989	30.3	32.9
1990	30.8	34.0			
1991	28.7	32.1			
1992	30.2	33.9			
1993	29.1	32.4			
1994	30.8	34.3			
1995	30.1	34.1			
1996	30.9	34.4			
1997	30.3	33.4			
1998	29.0	33.1	10 year mean		
1999	29.2	32.3	1990-1999	29.9	33.4
2000	30.4	33.9			
2001	30.4	33.5			
2002	30.4	33.3			
2003	30.9	33.7			
2004	30.1	32.8			
2005	29.4	33.0			
2006	31.3	35.2			
2007	30.4	34.2			
2008	31.3	34.2	10 year mean		
2009	30.4	33.0	2000-2009	30.5	33.7
2010	29.3	32.3			
2011	29.4	32.9			
2012	30.9	34.5			
2013	30.4	33.4			
2014	30.9	33.8			
2015	30.8	33.3			
2016	31.0	34.4			
2017	30.8	34.1	10 year mean		
2018	31.4	34.4	2009-2018	30.5	33.6

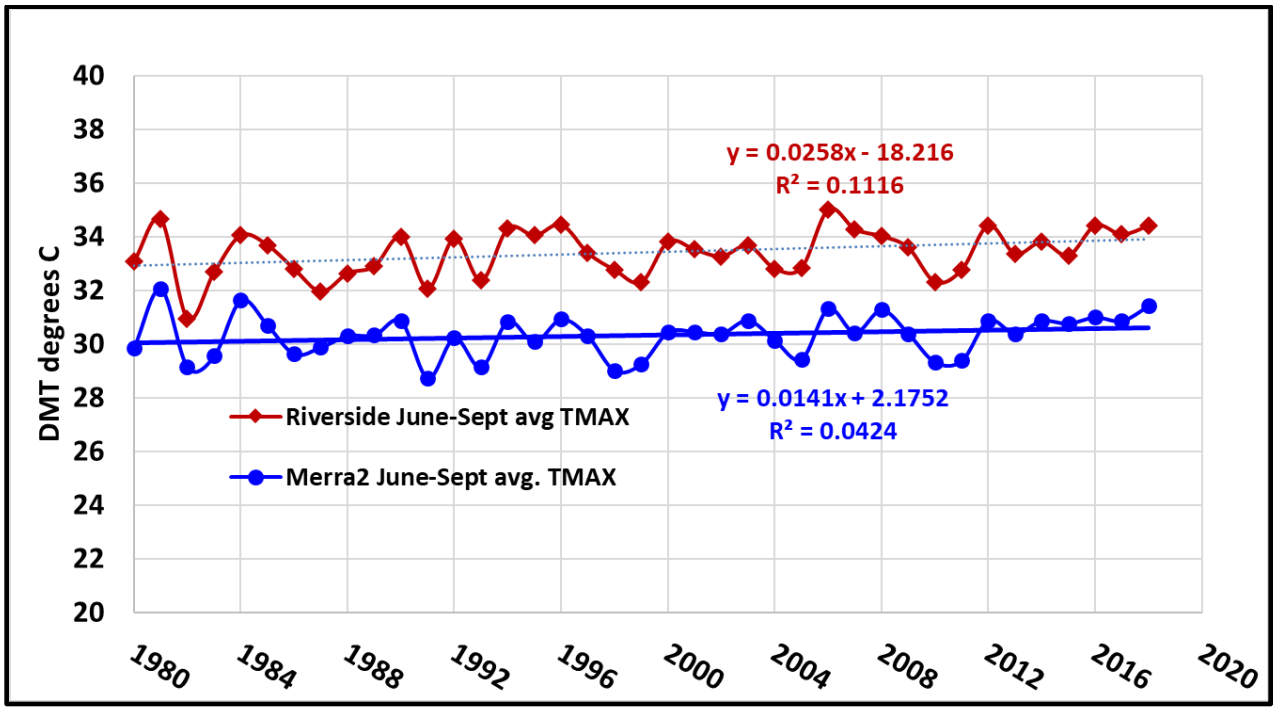

Figure 20. Average daily maximum temperature (°C) for June-September for Riverside and Merra-2. While both datasets show an increase, only the Riverside trend is statistically significant.

In addition to looking at change in the mean summer temperature, it is also important to look at the distribution of DMT values. Figures 21 and 22 show the distribution of DMT values for the first and last 4 years of this period (1980-2018).

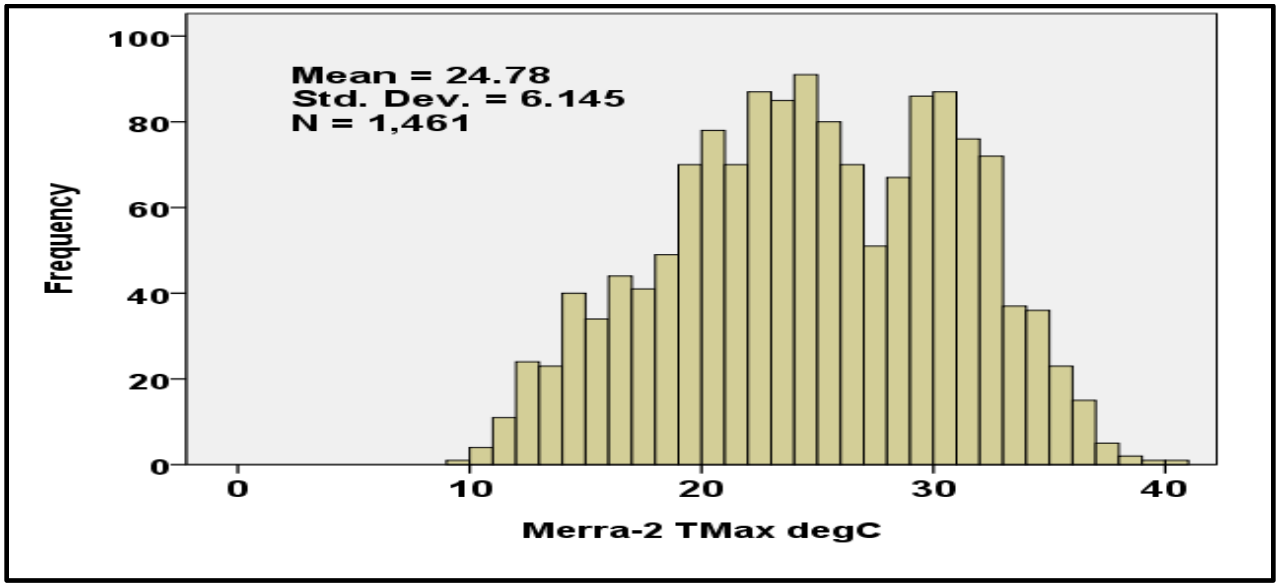

Figure 21. Distribution of annual DMT (ºC) for the years 2015-2018.

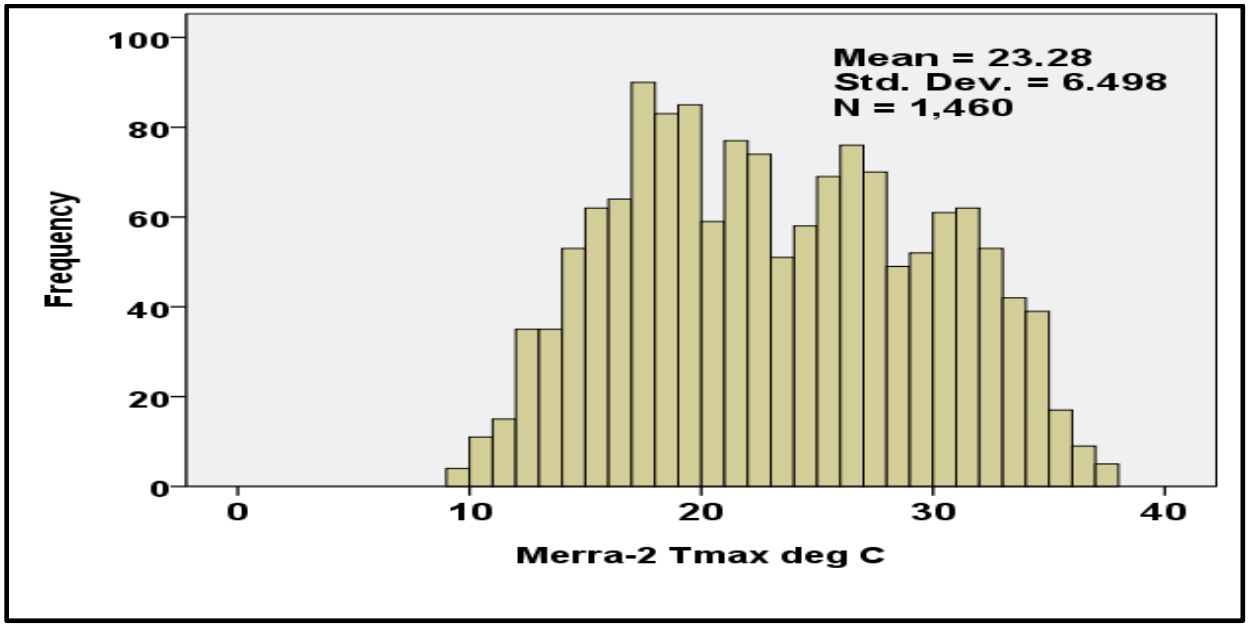

Figure 22. Distribution of annual DMT (ºC) for the years 1980-1983 from Merra-2.

The strong increase in the annual mean DMT (~1.5ºC in 35 years) compared to the values shown earlier likely reflects stronger increases due to global warming in winter, compared to summer. Figure 6 and 7 show the trend in DMT for the annual 95th and 98th percentile values. These are probably the most relevant metrics for O_3, since these represent the 18 and 7 hottest days each year, for the 95th and 98th percentile, respectively.

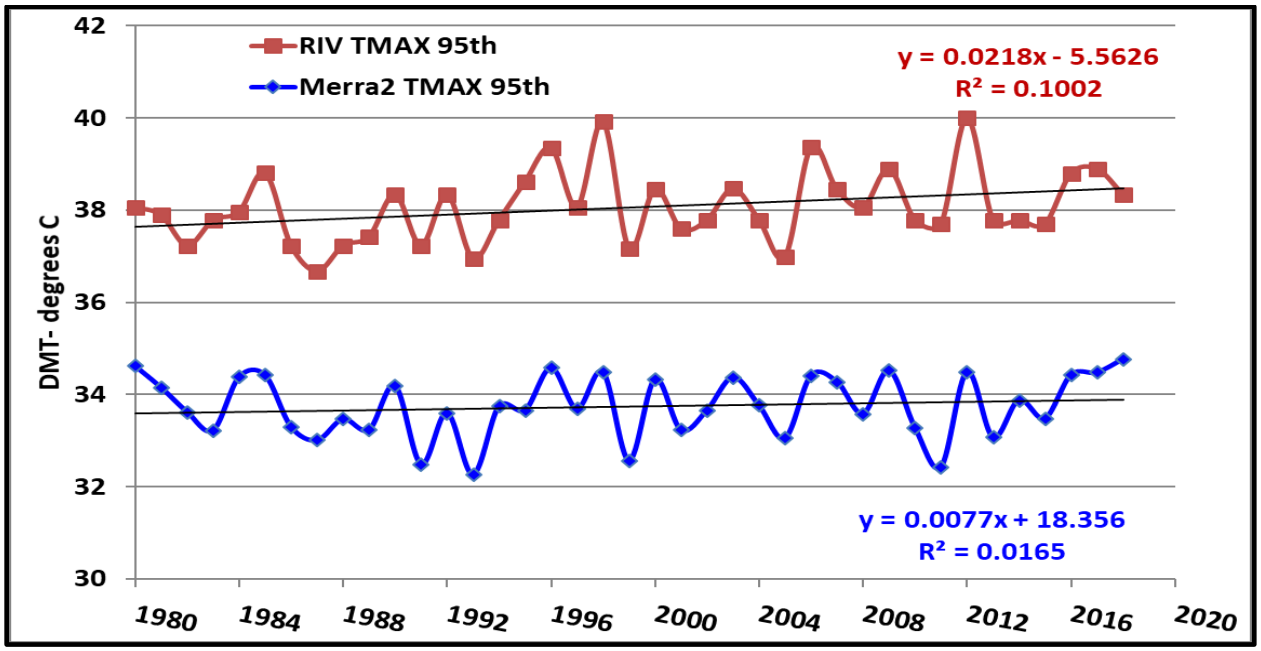

Figure 23. Trend in 95th percentiles of DMT (°C).

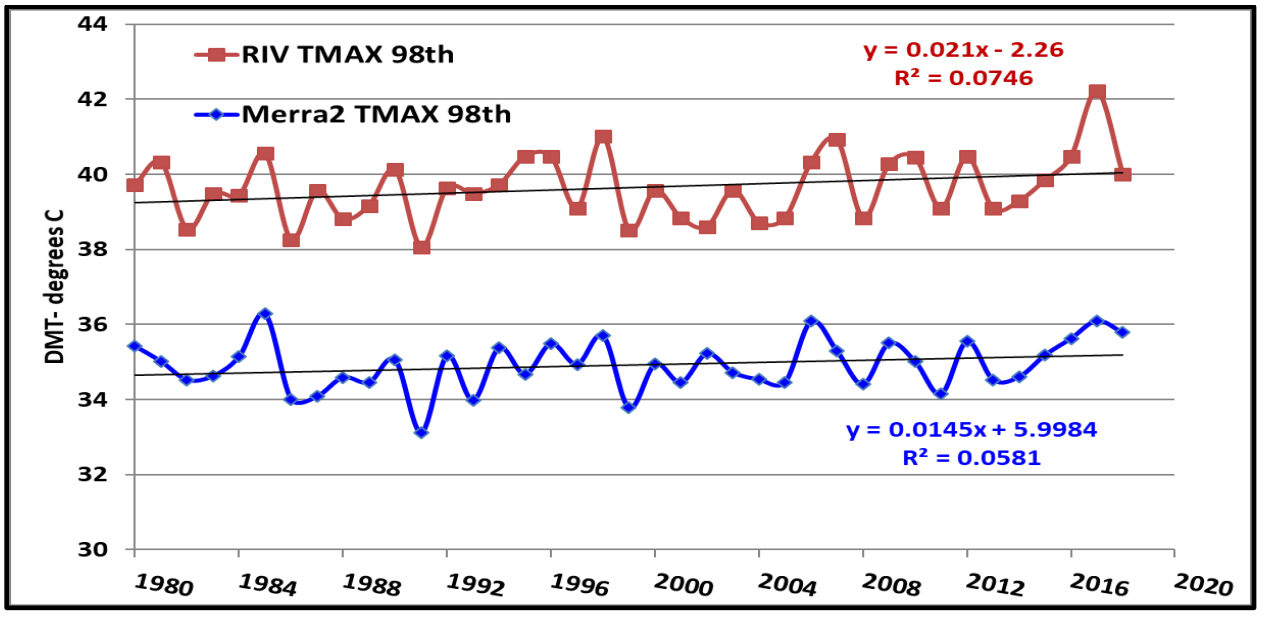

Figure 24. Trend in 98th percentile of DMT (°C).

The slopes of the 95th and 98th percentiles are very similar to slopes for the overall summer mean. So over this time period, the rise in the 95th and 98th percentile of DMT values are consistent with the steady upward climb due to climate change. For the 2016-2018 time period, there does not appear to be a stronger increase, with the exception of 2017, which saw a substantial jump in DMT, especially in the Riverside data. This certainly contributed to the increase in MDA8 values seen in 2017 (refer back to Figure 5).

Finally, I look at the temperature data from one last perspective, the fourth hottest day of the year. I choose this metric since it mirrors the policy relevant O_3 metric.

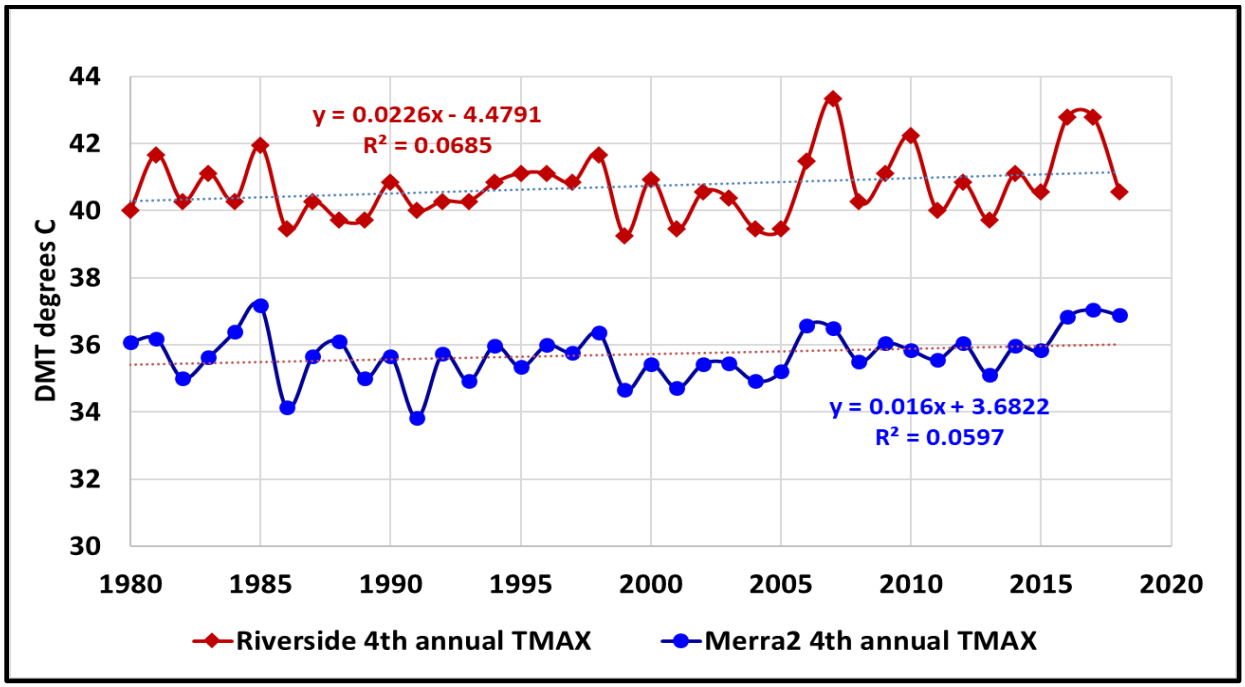

Figure 25. Trend in annual fourth highest DMT value for the Riverside and Merra-2 datasets. Linear trend lines are shown, but these are not statistically significant.

The fourth hottest day of each year (shown in Figure 25) is also consistent with the steady rise in temperatures due to climate change and the slopes are similar to those at 98th percentiles shown in Figure 24. So this analysis of temperature trends in the South Coast airsheds, indicates that the DMT is increasing by ~0.02^{o}C per year and that this increase is consistent across the mean and upper ends of the temperature distribution (e.g. 95th and 98th percentiles) as well as the fourth hottest day each year. This increase is also consistent with the pattern of global temperature rise, as reported by the NASA GISS analysis.

Next we want to evaluate how important this temperature trend has been on South Coast O_3 over the last few decades. For this, I need to re-examine the O_3-temperature sensitivity. Figure 26 shows the MDA8 values vs Riverside DMT, fit with both ordinary linear regression (OLR) and reduced major axis (RMA) regression lines.

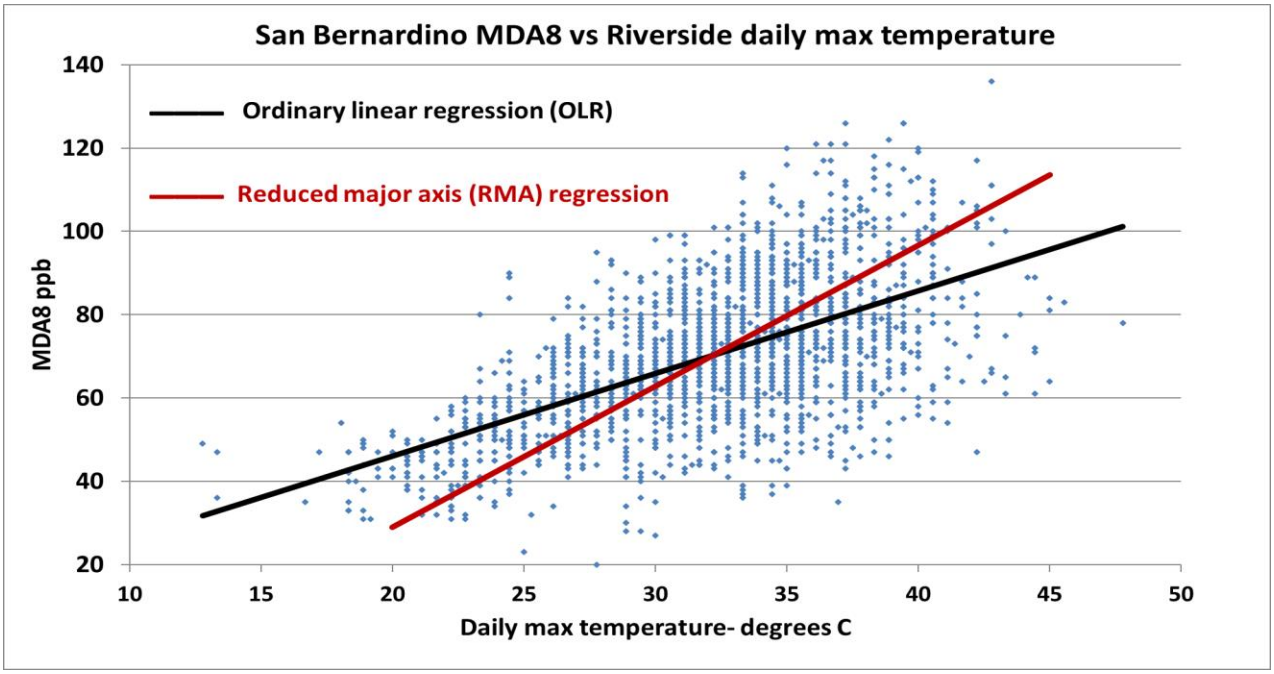

Figure 26. MDA8 values vs Riverside DMT (ºC) fit with both ordinary linear regression (OLR) and reduced major axis (RMA) regression lines.

OLR assumes errors in only the Y variable. This assumption is rarely correct for environmental analyses, but in practice, this only matters when the R^2 are modest (e.g. below 0.6). RMA regressions gives a better estimate of the true slope, as it considers errors in both the X and Y variables. For the plot above, the R^2 value is 0.35, so RMA regression is used to give a better estimate of the slope. Table 9 shows the OLR and RMA regression slopes for the MDA8 values from all sites using both the Riverside and Merra-2 DMT values. I also evaluated whether these slopes have changed significantly over the time span considered here (2006-2018) and there is no evidence for this.

Table 9. OLR and RMA regression slopes for the MDA8 values vs the Riverside and Merra-2 DMT values for May-September 2006-2018.

Slopes in ppb/ºC	SBO	RRO	POMO	GLO	VAFB	CRO
OLR Slope: MDA8/RivTmax	2.03	1.71	1.77	2.02	-0.41	1.56
OLR Slope: MDA8/MerraTmax	2.52	2.02	2.09	2.36	-0.63	2.22
RMA Slope: MDA8/RivTmax	3.46	2.94	2.92	3.23	1.65	3.52
RMA Slope: MDA8/MerraTmax	4.30	3.66	3.62	4.02	2.05	4.38

Using the RMA regressions, I find that the temperature sensitivity for the MDA8 values is between 2.9-4.4 ppb in the MDA8 per ^{o}C in daily max temperature (excluding VAFB). So the 0.02 ^{o}C/year increase in temperature corresponds to an increase in the average MDA8 of around 0.06-0.08 ppb/year or 0.6-0.8 ppb per decade. Note that my analysis also indicates that the extreme temperature days (95th and 98th percentiles) are going up at about the same rate as the overall mean (0.02 ^{o}C) so climate change, at present, has only a minor impact on the region's ability to meet the National Ambient Air Quality Standards (NAAQS).

It is important to note that the most recent Intergovernmental Panel on Climate Change (IPCC 2014) indicates that the rate of change in temperature may increase significantly, to ~0.04 ^{o}C/year. This rate of change will have a more significant impact on O_3 in the future. Steiner et al (2010) reports suppression of O_3 formation on days with very high daily max temperatures (above approximately 40 ^{o}C) for a number of sites across California. They claim that this could ameliorate, somewhat, the impacts of future climate change on O_3. I examined the data from this perspective. Figure 27 shows MDA8 values binned by the DMT. From this we can observe that at the highest DMT values, there is a flattening in the O_3 response and even, at some sites, a tendency for lower MDA8 values, similar to the findings reported by Steiner et al (2010). While this effect could be important in the future, at present, the temperature changes due to climate change are not yet large enough for this to matter. In summary, climate change has, so far, been a relatively minor contributor to the changes in O_3 concentrations seen in the South Coast and cannot explain the lack of progress in reaching lower ODVs.

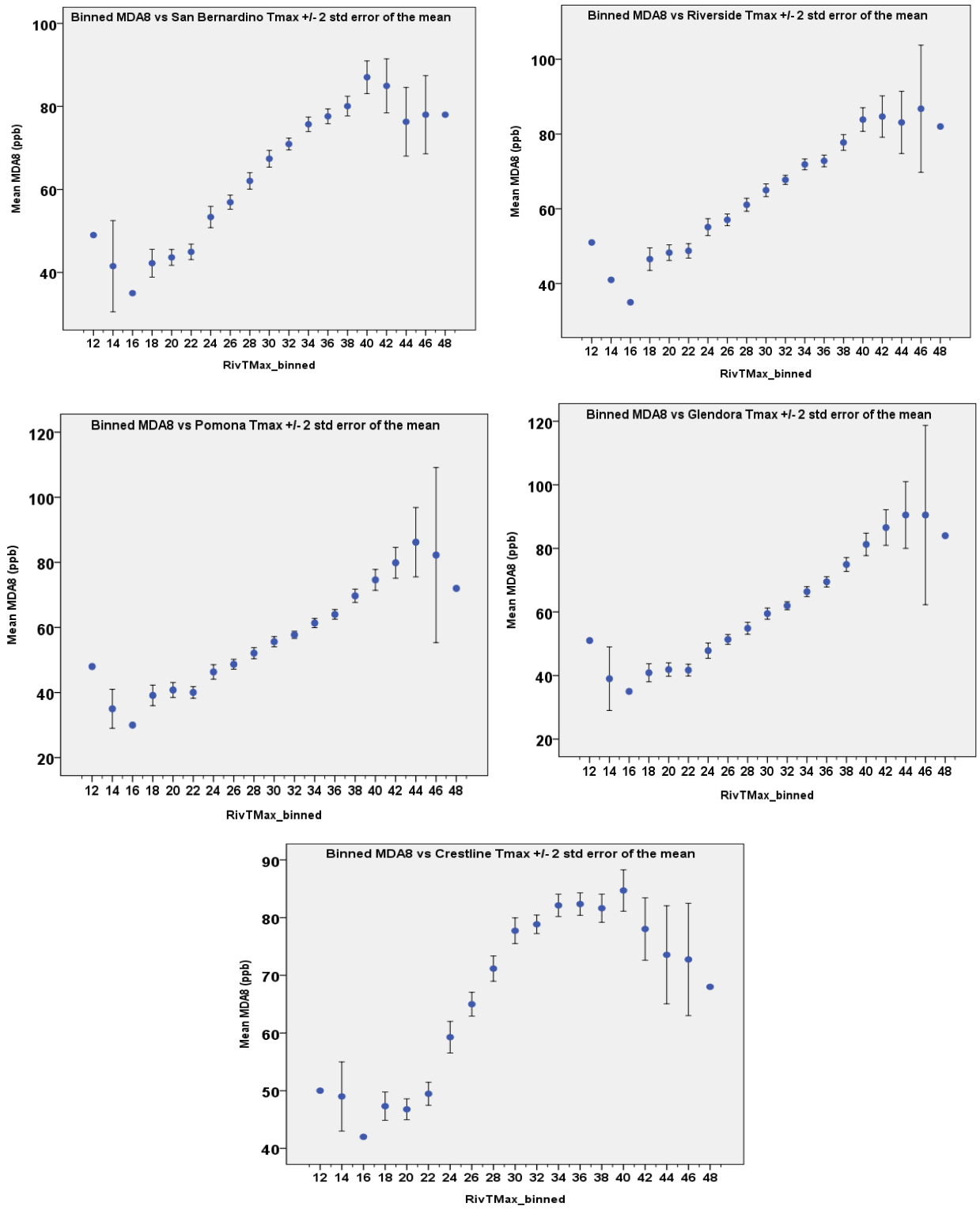

Figure 27. MDA8 values plotted by DMT in 2ºC bins for 5 sites. Error bars show 2 standard deviations of the mean for May-September 2006-2018.

5. Conclusions and suggestions for future research

In this project, I sought to understand the pattern and changes in the concentration of O_3 in the Los Angeles-Riverside/South Coast airshed. This region currently has the highest ODV in the country and is home to approximately 18 million people. While MDA8 O_3 concentrations have declined substantially from the extremely high values seen in the 1980-2000 period, since approximately 2010 there has been very little improvement, despite substantial reductions in emissions of O_3 precursors. The focus of this project was to understand possible causes for this lack of improvement. Three hypotheses were considered:

1. Recent O_3 concentrations have been enhanced due to changes in the photochemical environment driven by changes in the VOC/NOx ratio.
2. Recent O_3 concentrations have been enhanced due to an increase in the occurrence of wildfire smoke in the region.
3. Recent O_3 concentrations have been enhanced due to increased temperatures in the region, either due to random variations or climate change.

To evaluate these hypotheses I used a variety of tools including analysis of the O_3 and NOx patterns, development of Generalized Additive Models, identification of smoke days using satellite data and surface $PM_{2.5}$ observations and analysis of long-term meteorological data in the region. The time period of this analysis focused on 2000-2018. The GAMs were developed using data for 2006-2018. From this analysis, I have come to the following conclusions:

i. In the early part of this period (2006-2008), the highest number of high O_3 days was on weekends, when NOx concentrations were lowest. At present, the greatest number of high O_3 days are on weekdays. In contrast to the earlier period, Sunday now has the fewest high O_3 days and is the day with the lowest NOx concentrations. As NOx concentrations have declined on all days, this suggests that Sundays have transitioned to a NOx limited regime and weekdays are now at a VOC/NOx ratio that is near the optimum for O_3 production.

ii. NOx concentrations steadily declined until 2014, but have stagnated since then. This is in contrast to the CARB EI which shows a steady decline thru 2018. Between 2014 and 2018 the EI shows a 20% reduction whereas surface and satellite observations of NO_2 show essentially no change. This suggests that emissions have not declined since 2014.

iii. GAMs are effective tool to model and predict MDA8 in the South Coast airshed. The R^2 for the GAM predictions range from 0.67 to 0.76. The GAM has a lower predictive power for the Vandenberg AFB site ($R^2 = 0.53$), where concentrations are lower and local O_3 production is less important. Due to the changing photochemical environment, inclusion of interaction terms between predictors improves the GAM performance.

iv. Relatively high $PM_{2.5}$ in the airshed makes it difficult to clearly identify fire influence at the lower elevation (basin) sites, compared to the Crestline site. Thus impacts on the

MDA8 O_3 due to smoke can only be confidently detected at the Crestline site. At Crestline, the mean residual or extra O_3 due to smoke is 5.6 ppb for the MDA8. In 2016-2018, there were 29 detectable smoke days at Crestline. However even if all 29 days were excluded from consideration, the 2016-2018 design value would only change from 111 to 108 ppb. Thus while we can say that smoke has a modest influence on the MDA8 at Crestline, it does not appear to be a primary driver for the lack of decline in the ODV for the South Coast airshed.

v. Daily max temperature is an important driver for the daily variations in the MDA8 and due to climate the DMT is increasing by about 0.02^{o}C/year. This increase is consistent across the mean, 95th and 98th percentiles of the DMT values. This will increase the average MDA8 value by 0.06-0.08 ppb per year or 0.6-0.8 ppb per decade and thus has only a minor impact on the region's ability to meet the National Ambient Air Quality Standards (NAAQS).

The recent reductions in O_3 seen on Sundays, the day with the lowest NOx concentrations, demonstrates that continued NOx reductions are needed to reduce the ODV in the South Coast airshed. Weekday NOx levels are now similar to what they were on weekends 15 years ago and this is probably near the optimum VOC/NOx ratio for O_3 production. Given the strong decline in VOCs over the past several decades and the fact that biogenic VOCs are now a significant fraction of the total emissions (see Figure 2), further reductions in the ODV will likely only occur when NOx emissions are further reduced. Future research should focus on understanding the cause for the lack of decline in NOx concentrations since 2014. Our analysis suggests that the EI is presenting an overly optimistic view of the emissions reductions. This could be due to a variety of factors including population growth, changes in commuter patterns, changes in industrial emissions, changes in agricultural emissions, changes in biogenic emissions or other unknown causes. Our analysis suggests that a better understanding of the emission pattern and trends is needed to understand the trend in the ODV for the South Coast airshed.

6. **References**

Abatzoglou, J. T. & Williams, A. P. Impact of anthropogenic climate change on wildfire across western US forests. *Proc. Natl. Acad. Sci.* 113, 11770–11775, 2016.

Ashok, A.; Barrett, S. R. H. Adjoint-Based Computation of U.S.Nationwide Ozone Exposure Isopleths. Atmos. Environ., 133, 68−80, 2016.

Baidar, S., R. M. Hardesty, S.-W. Kim, A. O. Langford, H. Oetjen, C. J. Senff, M. Trainer, and R. Volkamer. Weakening of the weekend ozone effect over California's South Coast Air Basin, Geophys. Res. Lett., 42, 9457–9464, doi:10.1002/2015GL066419, 2015.

Baker, K. R.; Woody, M. C.; Tonnesen, G. S.; Hutzell, W.; Pye, H. O. T.; Beaver, M. R.; Pouliot, G.; Pierce, T. Contribution of regional-scale fire events to ozone and $PM_{2.5}$ air quality estimated by photochemical modeling approaches. Atmos. Environ. 140, 539-554, 2016.

Baker K.R., et al Photochemical model evaluation of 2013 California wildfire air quality impacts using surface, aircraft, and satellite data. Sci. Tot. Env., 637–638, 1137–1149, https://doi.org/10.1016/j.scitotenv.2018.05.048, 2018.

Buysse C.E. Kaulfus A. Nair U. and Jaffe D.A. Relationships between particulate matter, ozone, and nitrogen oxides during urban smoke events in the western US. Environ. Sci. Technol., DOI: 10.1021/acs.est.9b05241, 2019.

Cai, C., Avise, J., Kaduwela, A., DaMassa, J., Warneke, C., Gilman, J. B., et al. Simulating the weekly cycle of NO*x*-VOC-HO*x*-O3 photochemical system in the South Coast of California during CalNex-2010 campaign. *Journal of Geophysical Research: Atmospheres, 124*, 3532–3555. https://doi.org/10.1029/2018JD029859, 2019.

California Air Resources Board (CARB 2019), CEPAM: 2016 SIP - Standard Emission Tool Emission Projections By Summary Category, Base Year: 2012. https://www.arb.ca.gov/app/emsinv/fcemssumcat/fcemssumcat2016.php (Last accessed Dec. 21, 2019)

Camalier, L.; Cox, W.; Dolwick, P. The effects of meteorology on ozone in urban areas and their use in assessing ozone trends. Atmos. Environ., 41, (33), 7127-7137, 2007.

Dennison, P.E., Brewer, S.C., Arnold, J.D., Moritz, M.A. Large wildfire trends in the western United States, 1984–2011. Geophys. Res. Lett. 41, 2928–2933. https://doi.org/10.1002/2014GL059576, 2014.

Gelaro R. et al. The Modern-Era Retrospective Analysis for Research and Applications, Version 2 (MERRA-2). J. Clim., doi: 10.1175/JCLI-D-16-0758.1, 2017.

Gong X., Kaulfus A., Nair U. and Jaffe D.A. Quantifying O_3 impacts in urban areas due to wildfires using a Generalized Additive Model. Envir. Sci. Tech. DOI: 10.1021/acs.est.7b03130, 2017.

Gong X., Hong S. Jaffe D.A. Ozone in China: Spatial distribution and leading meteorological factors controlling O_3 in 16 Chinese cities. Aer. Air Qual. Res, DOI: 10.4209/aaqr.2017.10.0368, 2018.

Horne J.R. and Dabdub D., Impact of global climate change on ozone, particulate matter, and secondary organic aerosol concentrations in California: A model perturbation analysis. Atmospheric Environment 153, 1e17, 2017.

IPCC, 2014: Climate Change 2014: Synthesis Report. Contribution of Working Groups I, II and III to the Fifth Assessment Report of the Intergovernmental Panel on Climate Change [Core Writing Team, R.K. Pachauri and L.A. Meyer (eds.)]. IPCC, Geneva, Switzerland, 151 pp, 2014.

Jacob, D.J., and D.A. Winner. Effect of climate change on air quality. Atmospheric Environment 43(1): 51-63, 2009.

Jaffe, D.A. and Wigder, N.L., Ozone production from wildfires: A critical review. Atmos, Envir., doi: 10.1016/j.atmosenv. doi: 2011.11.063, 2012.

Jaffe DA, Cooper OR, Fiore AM, Henderson BH, Tonneson GS, Russell AG, Henze DK, Langford AO, Lin M and Moore T. Scientific assessment of background ozone over the U.S.: Implications for air quality management. Elem Sci Anth. 2018;6(1):56. doi:http://doi.org/10.1525/elementa.309, 2018.

Kaulfus, A.S., Nair, U., Jaffe, D.A., Christopher, S.A., and Goodrick, S. Biomass burning smoke climatology of the United States: Implications for particulate matter air quality, Environmental Science & Technology 50, 11731-11741, doi: 10.1021/acs.est.7b03292, 2017.

Kim, S.-W., et al. Modeling the weekly cycle of NOx and CO emissions and their impacts on O_3 in the Los Angeles-South Coast Air Basin during the CalNex 2010 field campaign, J. Geophys. Res. Atmos., 121, 1340–1360, doi:10.1002/2015JD024292, 2016.

Laing J.R. and Jaffe D.A. Wildfires Are Causing Extreme PM Concentrations in the Western United States. EM- The Magazine for Environmental Managers, AWMA , June, 2019

McClure C.D. and Jaffe D.A. Investigation of High Ozone Events due to Wildfire Smoke in an Urban Area. Atmos. Envir. https://doi.org/10.1016/j.atmosenv.2018.09.021, 2018.

McDonald, B. C., de Gouw, J. A., Gilman, J. B., Jathar, S. H., Akherati, A., Cappa, C. D., et al. Volatile chemical products emerging as largest petrochemical source of urban organic emissions. Science, 359(6377), 760–764, https://doi.org/10.1126/science.aaq0524, 2018.

Pollack, I. B., T. B. Ryerson, M. Trainer, J. A. Neuman, J. M. Roberts, and D. D. Parrish. Trends in ozone, its precursors, and related secondary oxidation products in Los Angeles, California: A synthesis of measurements from 1960 to 2010, J. Geophys. Res. Atmos., 118, 5893–5911, doi:10.1002/jgrd.50472, 2013.

Pusede S.E., Steiner A.L. and Cohen R.C. Temperature and Recent Trends in the Chemistry of Continental Surface Ozone. Chem. Rev. Chem. Rev., 115, 3898−3918, DOI: 10.1021/cr5006815, 2015.

Qian Y., Lucas R.F., Henneman J.A., Mulholland A., and Russell A.G. Empirical Development of Ozone Isopleths: Applications to Los Angeles. Environ. Sci. Technol. Lett., 65, 294-299, https://doi.org/10.1021/acs.estlett.9b00160, 2019.

Silvern, R. F., Jacob, D. J., Mickley, L. J., Sulprizio, M. P., Travis, K. R., Marais, E. A., Cohen, R. C., Laughner, J. L., Choi, S., Joiner, J., and Lamsal, L. N.: Using satellite observations of tropospheric NO_2 columns to infer long-term trends in US NO_x emissions: the importance of accounting for the free tropospheric NO_2 background, Atmos. Chem. Phys., 19, 8863–8878, https://doi.org/10.5194/acp-19-8863-2019, 2019.

Steiner A., Davis A.J. Sillman S., Owen, R.C. Michalak A.M. and Fiore A.M. Observed suppression of ozone formation at extremely high temperatures due to chemical and biophysical feedbacks. Proc. Natl. Acad. Sci. 107 (46) 19685-19690; https://doi.org/10.1073/pnas.1008336107, 2010.

Westerling, A. L. Increasing western US forest wildfire activity: sensitivity to changes in the timing of spring. Phil. Trans. R. Soc. B 371: 1696, 2016.

7. Appendix

The following graphs show results and quality control output from the mgcv package in R. For this, I use the San Bernardino training dataset as an example. The model results are stored in the variable MS.

```
> summary(MS)

Family: gaussian
Link function: identity

Formula:
SBO ~ s(TrDIST12, by = TrQ12) + s(Y, DOW) + s(Y, RivNO2) + s(UV,
    bs = "cr", k = 10) + s(T850M, bs = "cr", k = 10) +
    s(T850A, bs = "cr", k = 10) + s(RIVTMAX, bs = "cr",
    k = 10) + s(DOY, bs = "cr", k = 10) + s(THCKA, bs = "cr",
    k = 10) + DOW

Parametric coefficients:
            Estimate Std. Error t value Pr(>|t|)
(Intercept)  16.9049     0.3473   48.68   <2e-16 ***
DOW          13.3149     0.1025  129.94   <2e-16 ***
---
Signif. codes:  0 ‘***’ 0.001 ‘**’ 0.01 ‘*’ 0.05 ‘.’ 0.1 ‘ ’ 1

Approximate significance of smooth terms:
                       edf Ref.df       F  p-value
s(TrDIST12):TrQ12NE  4.640  5.525   4.167 0.000762 ***
s(TrDIST12):TrQ12NW  1.894  2.386   4.320 0.012649 *
s(TrDIST12):TrQ12SE  1.452  1.782   0.785 0.545361
s(TrDIST12):TrQ12SW  4.359  5.294   3.874 0.001329 **
s(Y,DOW)            26.337 28.417 292.626  < 2e-16 ***
s(Y,RivNO2)          8.960 12.565   1.507 0.103617
s(UV)                8.199  8.751  20.047  < 2e-16 ***
s(T850M)             1.000  1.000  12.560 0.000407 ***
s(T850A)             5.556  6.746  34.629  < 2e-16 ***
s(RIVTMAX)           7.879  8.665  13.362  < 2e-16 ***
s(DOY)               6.871  7.963  13.531  < 2e-16 ***
s(THCKA)             2.476  3.253   2.207 0.080407 .
---
Signif. codes:  0 ‘***’ 0.001 ‘**’ 0.01 ‘*’ 0.05 ‘.’ 0.1 ‘ ’ 1

Rank: 148/149
R-sq.(adj) =  0.744   Deviance explained = 75.8%
GCV = 83.062  Scale est. = 78.295    n = 1408
```

```
> gam.check(MS)
```

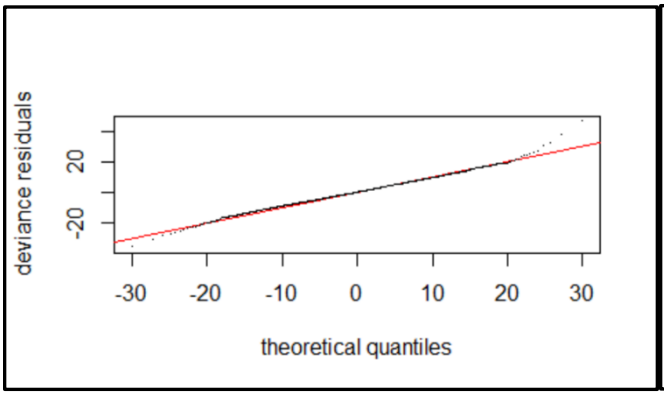
deviance residuals
-20
20
-30
-20
-10
0
10
20
30
theoretical quantiles

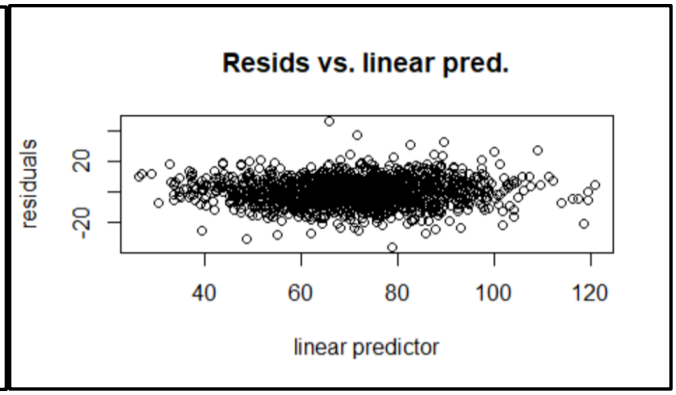
Resids vs. linear pred.
residuals
-20
20
40
60
80
100
120
linear predictor

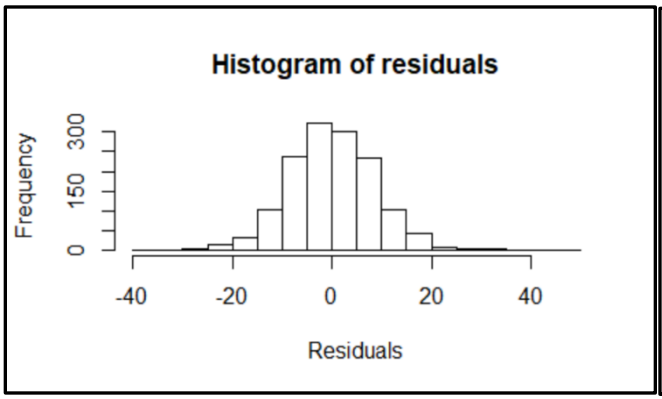
Histogram of residuals
Frequency
0
150
300
-40
-20
0
20
40
Residuals

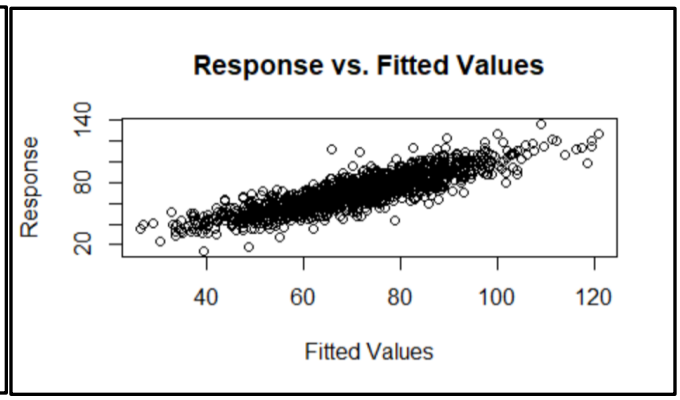
Response vs. Fitted Values
Response
20
80
140
40
60
80
100
120
Fitted Values

```
> plot(MS, scale=0)

#Individual spline plots. In each case, the y-axis show that variables
#contribution to the predictand (San Bernardino MDA8 O3).  Marks on
#the x-axis #indicate the density of points and the dashed lines show
#the 2 standard error boundary about the spline fit. Note that results
#can be counter intuitive near the extremes when there are few points.
```

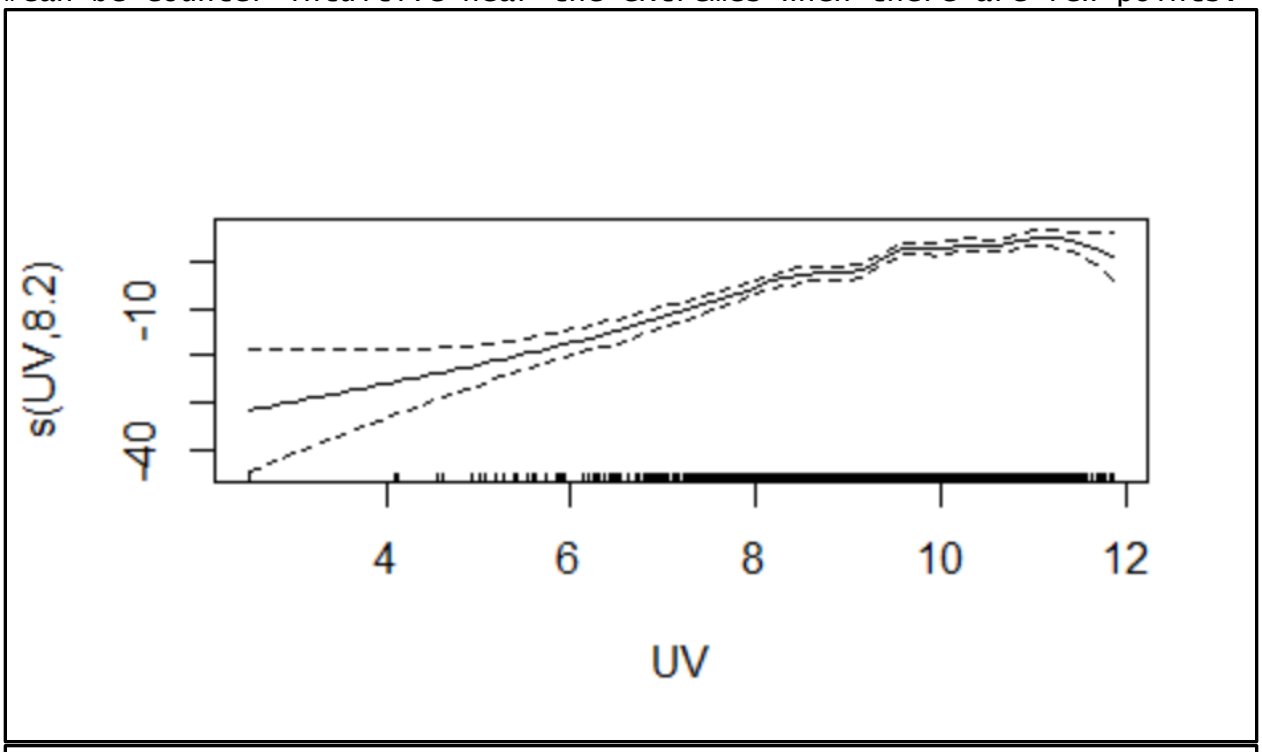

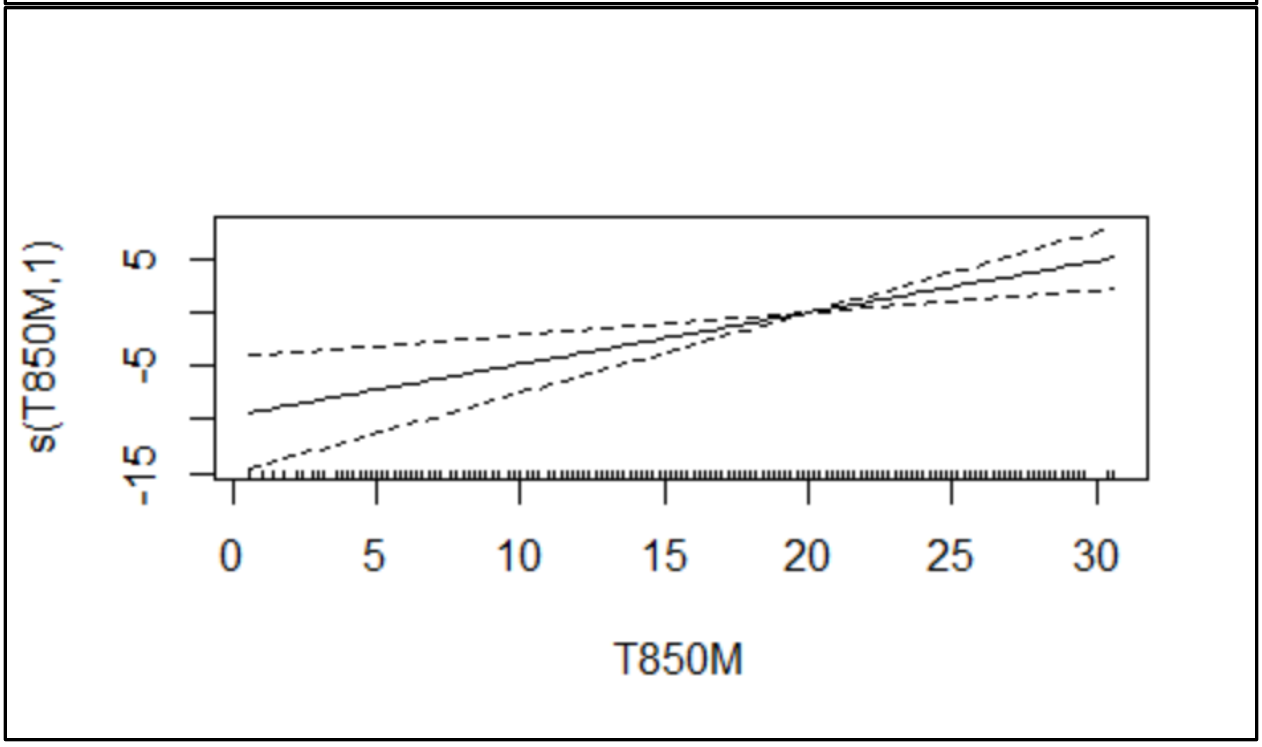

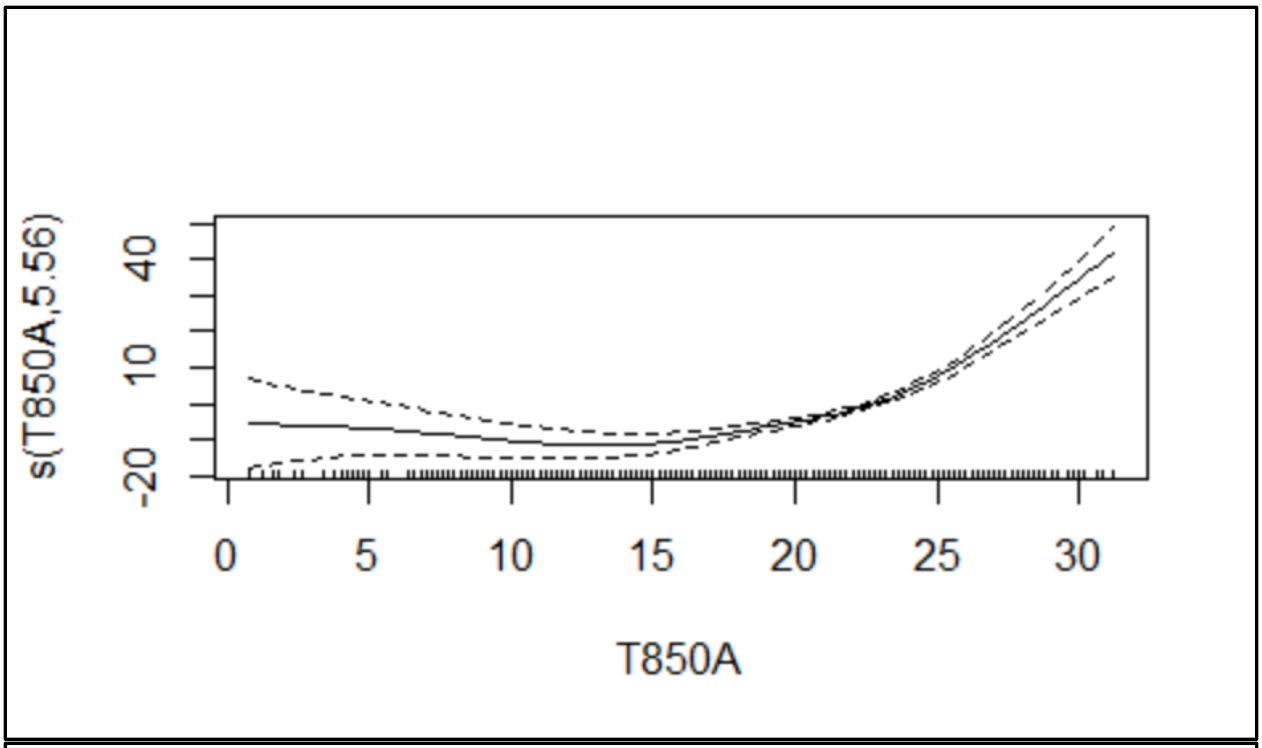
s(T850A,5.56)
-20
10
40
0
5
10
15
20
25
30
T850A

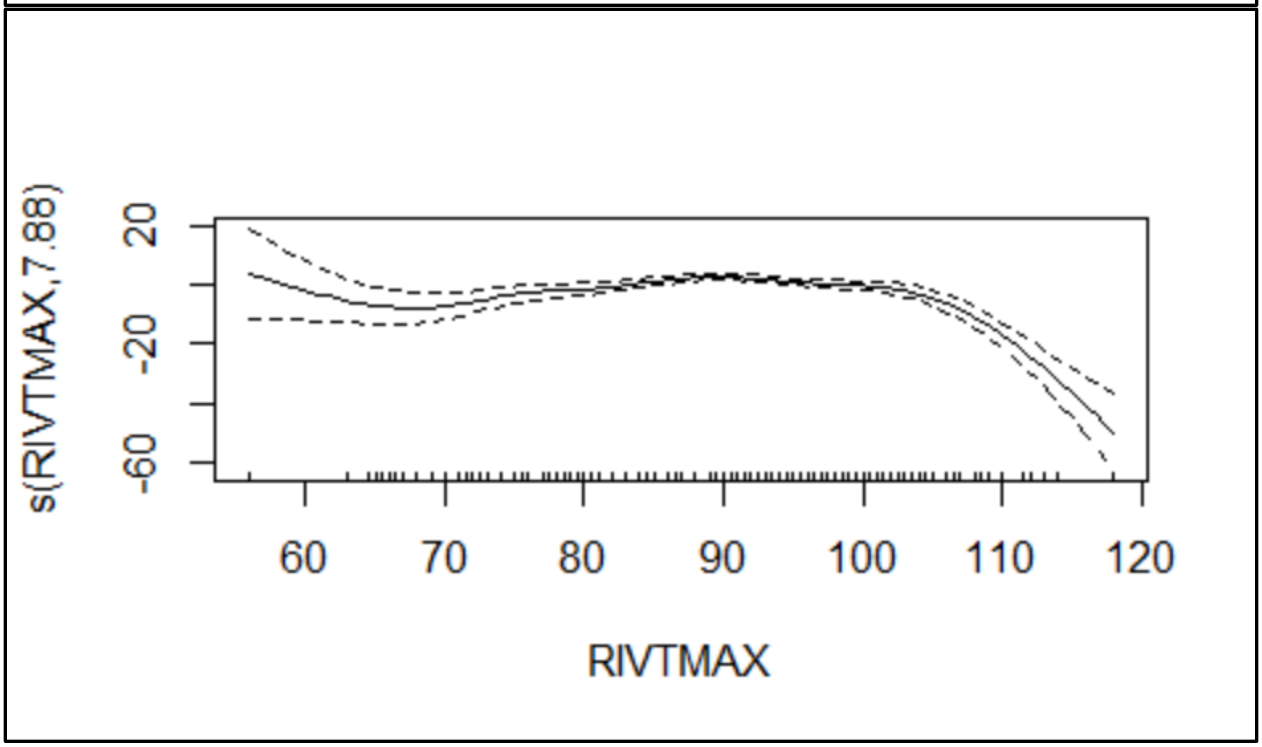
s(RIVTMAX,7.88)
-60
-20
20
60
70
80
90
100
110
120
RIVTMAX

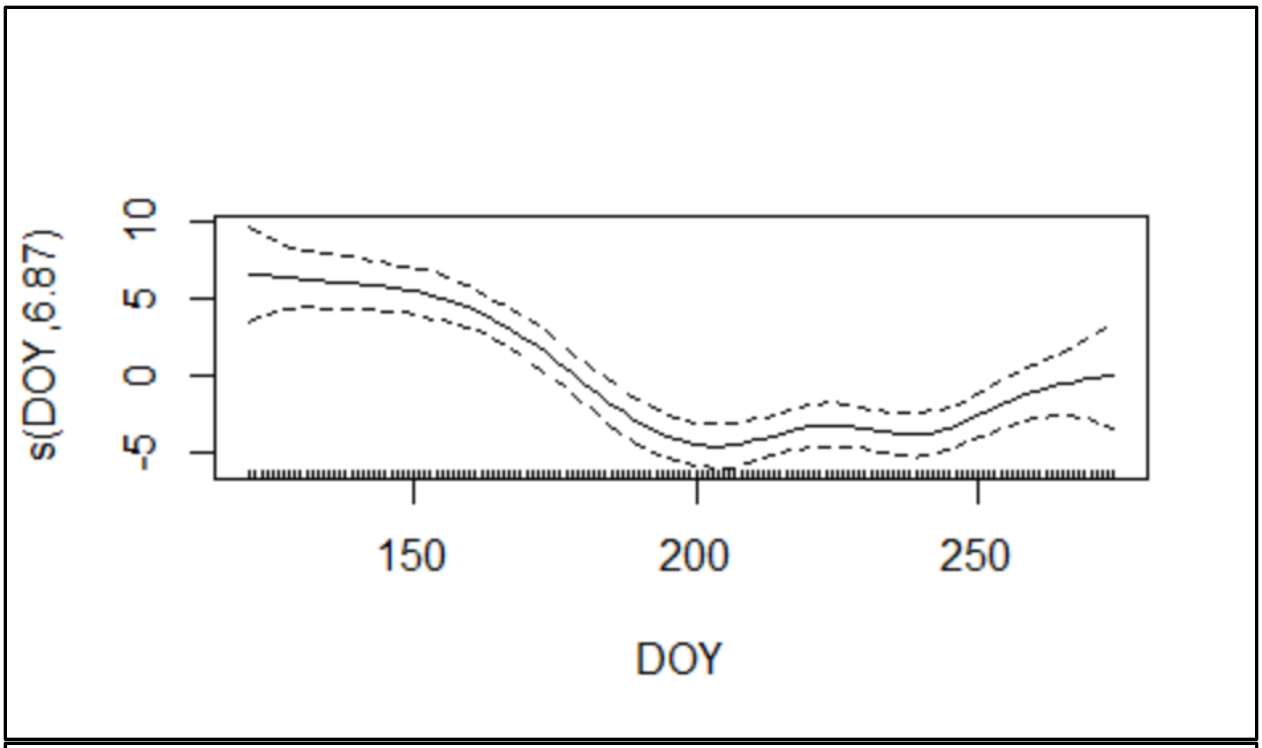
s(DOY,6.87)
-5
0
5
10
150
200
250
DOY

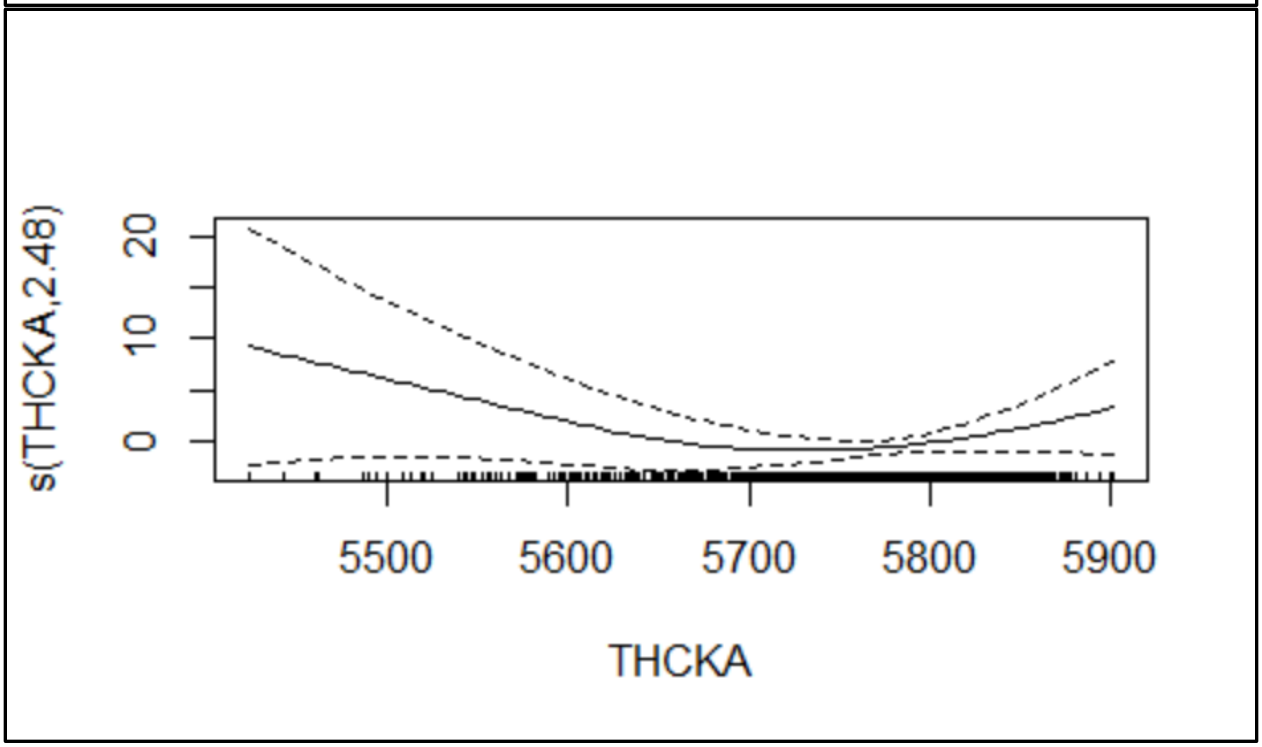
s(THCKA,2.48)
0
10
20
5500
5600
5700
5800
5900
THCKA

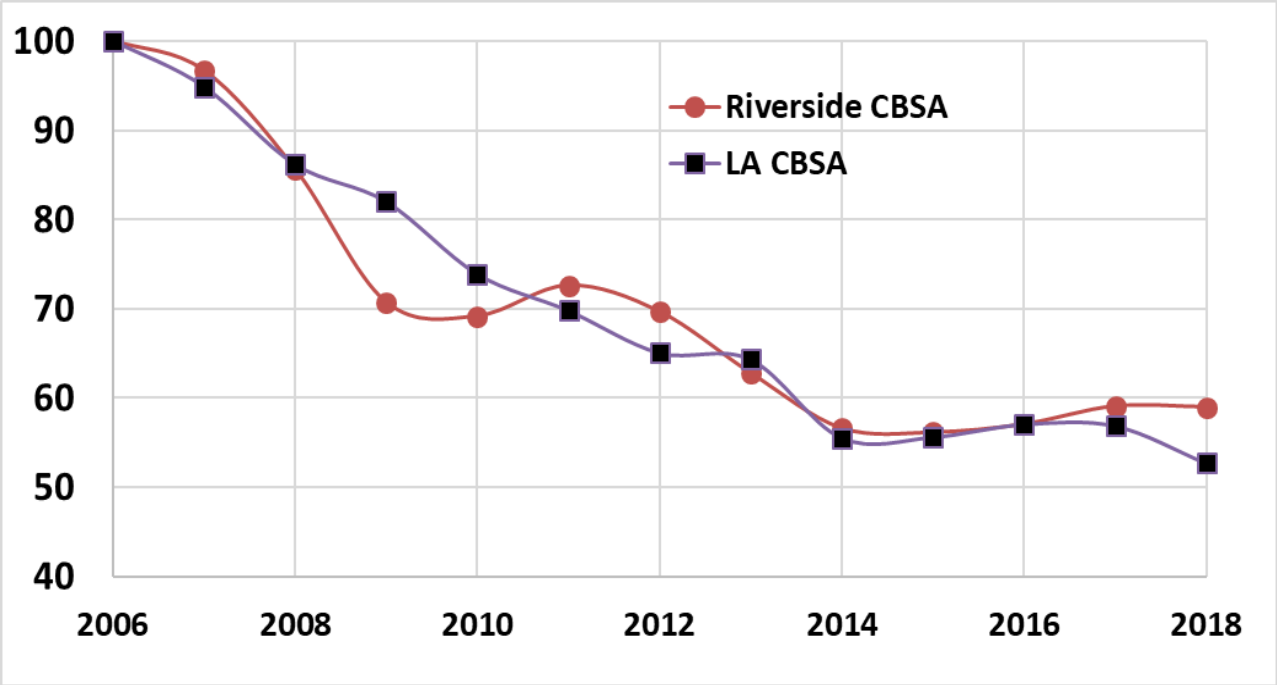

Figure A1. Change in summer (June-August) surface NO2 observations (1-hour daily maximum) from monitors in the Los Angeles and Riverside CBSAs. Only sites with near continuous records (for the Los Angeles CBSA there are 14 sites and for the Riverside CBSA there are 8 sites). Values are normalized to a 2006 value of 100.

Table A1: Recent changes in summer (June-August) average NO_2 (ppb) for individual monitors in the Riverside and Los Angeles MSAs.

AQS monitor ID	Avg. summer NO_2 concentration (ppb), 2014-2015	Avg. summer NO_2 concentration (ppb), 2017-2018	% Change
Riverside MSA			
60650009	5.8	5.6	-3.6
60650012	18.6	20.6	+10.6
60651016	8.5	9.1	+6.4
60655001	10.4	10.4	+0.1
60658001	18.6	18.8	+0.9
60658005	16.5	16.1	-2.9
60659001	15.0	15.6	+4.3
60710001	34.1	36.1	+5.7
60710026	40.4	36.8	-8.9
60710027	46.0	40.2	-12.6
60710306	25.0	28.8	15.0
60711004	24.5	23.3	-4.6
60711234	16.8	15.3	-8.9
60712002	31.6	31.6	-0.1
60719004	25.5	25.7	0.5
		Riverside MSA average	**+0.1%**
Los Angeles MSA			
60370002	25.0	22.9	-8.7
60370016	20.8	18.1	-13.2
60370113	14.6	15.0	+2.5
60371103	27.4	25.7	-6.0
60371201	17.4	16.5	-5.1
60371302	17.2	17.0	-1.1
60371602	21.7	22.0	+1.3
60371701	27.6	26.9	-2.5
60372005	19.4	18.2	-6.1
60374006	22.2	20.8	-6.1
60374008	32.0	28.4	-11.1
60375005	13.2	12.9	-2.5
60376012	21.5	20.4	-4.8
60590007	12.8	11.8	-8.2
60590008	28.4	23.7	-16.6
60591003	8.5	7.1	-16.2
60595001	15.0	13.8	-7.5
		Los Angeles MSA average	**-6.6%**